doi.org/10.26434/chemrxiv.8967941.v2

Structure-Based Design of a Macrocyclic PROTAC

Andrea Testa, Scott J. Hughes, Xavier Lucas, Jane E. Wright, Alessio Ciulli

Submitted date: 12/11/2019 • Posted date: 20/11/2019

Citation information: Testa, Andrea; Hughes, Scott J.; Lucas, Xavier; E. Wright, Jane; Ciulli, Alessio (2019): Structure-Based Design of a Macrocyclic PROTAC. ChemRxiv. Preprint.
https://doi.org/10.26434/chemrxiv.8967941.v2

Constraining a molecule in its bioactive conformation via macrocyclization represents an attractive strategy to rationally design functional chemical probes. While this approach has been applied to enzyme inhibitors or receptor antagonists, to date it remains unprecedented for bifunctional molecules that bring proteins together, such as PROTAC degraders. Here, we report the design and synthesis of a first macrocyclic PROTAC by adding a second cyclizing linker to the BET degrader MZ1. A co-crystal structure of macroPROTAC-1 bound in a ternary complex with VHL and the second Brd4 bromodomain validated the rational design. Biophysical studies revealed enhanced discrimination between the second and the first bromodomains of BET proteins. Despite a 12-fold loss of binary binding affinity for Brd4, macroPROTAC-1 exhibited cellular activity comparable to MZ1. Our findings support macrocyclization as an advantageous strategy to enhance PROTAC degradation potency and selectivity between homologous targets.

File list (2)

Structure-Based Design of a Macrocyclic PROTAC

Andrea Testa, Scott J. Hughes, Xavier Lucas, Jane E. Wright, Alessio Ciulli*

Division of Biological Chemistry and Drug Discovery, School of Life Sciences, University of Dundee, Dow Street, Dundee, DD1 5EH, Scotland, United Kingdom

* E-mail: a.ciulli@dundee.ac.uk

ORCID ID: 0000-0002-8654-1670

Homepage: http://www.lifesci.dundee.ac.uk/groups/alessio-ciulli/

Keywords: proteolysis targeting chimeras (PROTACs), macrocycles, drug design, protein-protein interactions, protein structures

Supporting information for this article is given at the end of the document.

Abstract

Constraining a molecule in its bioactive conformation via macrocyclization represents an attractive strategy to rationally design functional chemical probes. While this approach has been applied to enzyme inhibitors or receptor antagonists, to date it remains unprecedented for bifunctional molecules that bring proteins together, such as PROTAC degraders. Here, we report the design and synthesis of a first macrocyclic PROTAC by adding a second cyclizing linker to the BET degrader MZ1. A co-crystal structure of macroPROTAC-1 bound in a ternary complex with VHL and the second Brd4 bromodomain validated the rational design. Biophysical studies revealed enhanced discrimination between the second and the first bromodomains of BET proteins. Despite a 12-fold loss of binary binding affinity for Brd4, macroPROTAC-1 exhibited cellular activity comparable to MZ1. Our findings support macrocyclization as an advantageous strategy to enhance PROTAC degradation potency and selectivity between homologous targets.

Table of Content Graphics

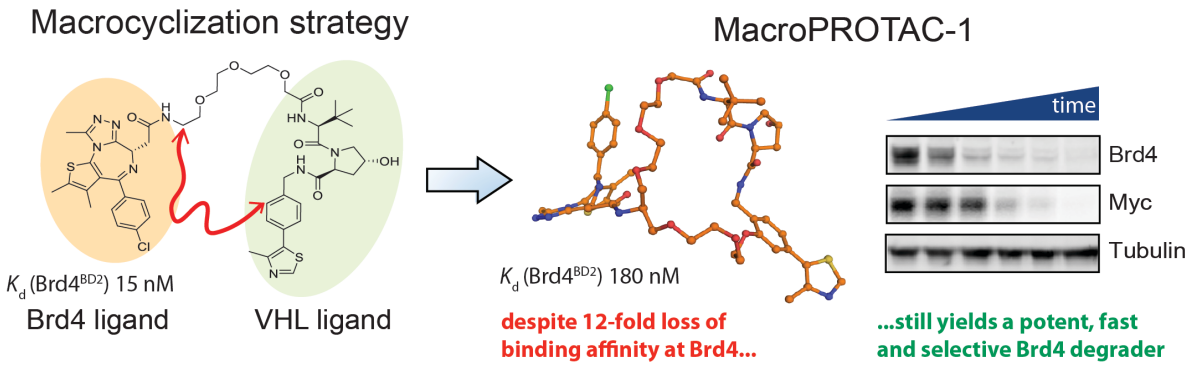

Targeted protein degradation is a powerful new modality of chemical biology and drug discovery.[1,2] PROTACs are bifunctional molecules composed of a ligand for a target protein of interest, and a ligand for an E3 ubiquitin ligase, joined by a flexible linker. Recruitment of a protein close to an E3 ligase hijacks the ligase catalytic activity, leading to the tagging of the target protein by ubiquitination and subsequent proteasomal degradation.[3-5] PROTACs are emerging as attractive chemical probes and therapeutics, defined by a catalytic and sub-stoichiometric rather than occupancy-based mode of action, leading to an extended duration of action.[6-9] Due to their different mechanism of action via formation of a ternary complex species, PROTACs have the potential to pharmacologically differentiate from inhibitors and to more effectively impact biology and disease, including targeting proteins that have proven intractable to other approaches.

Structural and biophysical investigation of ternary complexes from our laboratory revealed that proximity-induced formation of *de novo* interactions within the ternary complex are an important feature of the PROTAC mode of action.[10] Neomorphic interactions include protein-protein interactions (PPIs) between the ligase and the target, which can lead to formation of cooperative and stable ternary complexes.[11] These characteristics of the ternary complex, albeit not strictly essential for PROTAC-mediated protein degradation,[12,13] are important because they can increase the population of the complex (the key Michaelis-Menten species in the PROTAC-mediated catalytic process) and contribute to enhance its thermodynamic stability and kinetic dissociative half-life.[10,14,15] These features in turn enhance the catalytic efficiency of the process, leading to greater levels of target ubiquitination, and consequently faster and more prolonged target degradation.[15,16] Because the PROTAC-induced PPIs involve less-conserved regions outside of the ligand binding pocket, PROTACs made of promiscuous or non-selective target ligands can discriminate between highly homologous target proteins in a way not achievable with the parent inhibitors alone.[7,10,13,15,17,18]

Knowledge of the PROTAC binding mode in a ternary complex, ideally from co-crystal structures, provide an opportunity to rationally design compounds to better fit and stabilize the newly created interface within the ternary complex, using structure-based drug design.[10,13,19,20] Our first crystal structure of the PROTAC MZ1 in complex with the E3 ligase VHL and its target Brd4 bromodomain revealed that the two ligand moieties of MZ1 (the VHL ligand VH032 and BET inhibitor JQ1, respectively) lay in close spatial proximity within the ternary complexes. We thus imagined that a macrocyclic PROTAC could be

designed based on the crystal structure as a strategy to lock the PROTAC conformation in the bound state. Macrocyclization is expected to reduce the energetic penalty to adopt the bound state through conformational restriction.[21,22] As such, macrocycles provide privileged scaffolds to target PPIs and protein surfaces, amongst other challenging targets.[23-25] For example, the archetypal macrolide natural products cyclosporine and rapamycin are macrocyclic molecules that act as molecular glues to induce a ternary complex.[26,27] To the best of our knowledge, however, the exemplification of macrocylization as a strategy for PROTAC design, or more generally to bias recruitment of proteins together, remain unprecedented. Here we provide first proof-of-concept validation of the approach with a macrocyclic PROTAC. The design strategy was aided by computational calculations and molecular dynamics (MD) simulations based on the MZ1 ternary complex crystal structure. Macrocyclization was achieved by adding a second linker to "close a circle" between the two ligand moieties of MZ1. Using isothermal titration calorimetry (ITC), fluorescence polarization (FP) and X-ray crystallography, we show that macroPROTAC-1 better discriminates between recruitment of the second and the first BET bromodomains to VHL. Despite an >10-fold loss in binary binding affinity for Brd4, macroPROTAC-1 exhibits rapid and potent intracellular degradation of Brd4, and cytotoxicity in BET-sensitive cancer cell lines that are comparable to MZ1.

Inspired and guided by the crystal structure of the ternary complex between our BET degrader MZ1, VHL and $Brd4^{BD2}$ [10], we designed a series of macrocyclic PROTACs with the aim to "lock" the PROTAC in the bound conformation (Figure 1A). We hypothesized that macrocyclization would increase the energetic bias towards the 'productive' PROTAC ternary complex, relative to either non-productive ternary complexes, binary complexes or free in solution. Our approach to cyclize MZ1 relied upon identifying a suitable vector and linker that would retain the binding mode of the linear compound and at the same time maintain the induced PPIs that contribute to forming a stable and cooperative ternary complex that underpins the preferential degradation of BRD4.[10,15] Two vectors connecting a phenolic group on the VHL ligand to the same carbon of the first PEG unit of the MZ1 linker were explored (vectors A and B, Figure 1B).

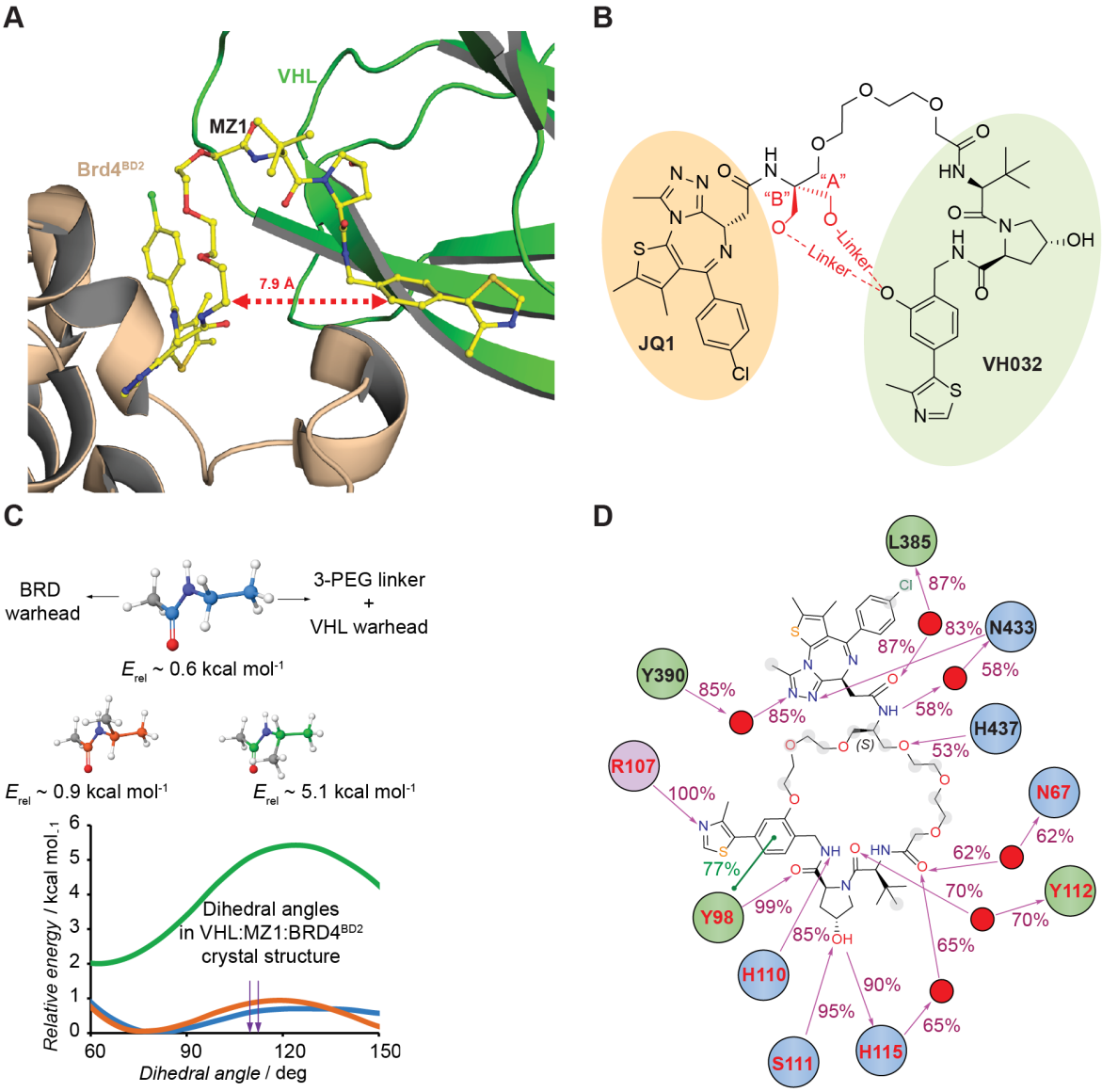

Figure 1. Structure based designed of macrocyclic PROTAC **1**. (A) Crystal structure of MZ1 in complex with Brd4^{BD2} and VHL-EloB-EloC shows MZ1 in a horseshoe shape, suggesting potential for cyclization (PDB code 5T35)[10]. (B) the two cyclization vectors "A" and "B" investigated computationally in this study. In black the chemical structure of MZ1, in red the additional liker. (C) Torsional energy profiling along the alkylamide dihedral of N-ethylacetamide (blue) and N-isopropylacetamide (orange and green), as surrogates of the chemical environment in the linker of MZ1 and its macrocyclic derivatives. (D) Chemical structure of **1** and its non-covalent interactions with VHL (residues in red), BRD4^{BD2} (residues in black) and water (red spheres), as observed during the last 50 ns of a 200 ns MD simulation of the VHL:**1**:BRD4^{BD2} ternary complex. The percentage of time spent in the interaction is shown. Charged, polar, and hydrophobic amino acids are colored in purple, blue, and green, respectively, and the solvent-exposure of atoms in **1** is highlighted in a gray shadow.

We first studied computationally the potential energy strain introduced by alkylation in vectors A and B in the JQ1-amide (Figure 1B), using the model compound *N*-ethylacetamide (Figure 1C).[28] We observed that the alkylamide torsion angles in the crystal structure of

MZ1 (110º and 112º)[10] are low-energy states in the surrogate *N*-ethylacetamide. Alkylation at vector A would force the amide to an eclipsed conformer, for which we found an energy penalty of ~ 5 kcal/mol. This modification would prevent the adoption of the crystallographic pose of the MZ1 linker, thereby disrupting the binding mode. We therefore deemed a derivatization from vector B to be more suitable. Molecular modelling studies were performed on derivatives **1** and **2** (supplementary figure S1A) cyclized from vector B with a linker comprising 3 and 2 PEG units, respectively. The modelling indicated that a 2-PEG linker, as in compound **2** (supplementary figure S1A), would be too short to cover the distance between the two attachment points and would impair binding of the MZ1 core (supplementary figure S1B). In contrast, a linker comprising 3 PEG units (compound **1,** supplementary figure S1A) could be well accommodated in the cavity formed between the proteins (supplementary figure S1C). We next performed molecular dynamics (MD) simulations of **1** bound to VHL and $BRD4^{BD2}$ in order to investigate the behavior of the ternary system in solution. The ternary complex remained stable throughout the simulation, with retention of the binding mode for the MZ1 portion of **1** and conservation of the interprotein and protein–PROTAC contacts observed in the VHL:MZ1:$BRD4^{BD2}$ structure (Supplementary figures S2 and S3). Crucially, the simulations suggested that macrocyclization was compatible with key polar interactions at each end of the new linker, including the water-mediated interaction of the JQ1-amide with $N433^{BRD4(BD2)}$, the H-bond of the oxygen atom in the first PEG unit in MZ1 with $H437^{BRD4(BD2)}$, and the H-bond with $Y98^{VHL}$ (Figure 1D). Only a very modest shortening between the attachment points was observed in the macrocycle (7.7 ± 0.3 Å, supplementary figure S2A) compared to MZ1 (8.1 Å),[10] as well as the formation of a stable water network at the proteins–PROTAC interface contributed by polar interactions with each partner (supplementary figure S3B). Thus, we selected **1** as the target macrocyclic derivative of MZ1 for synthesis.

In order to synthetically achieve our macrocyclic PROTAC **1**, a bespoke linker able to connect the BET ligand to the two different attachment points on the VHL ligand needed to be designed. We envisaged a retrosynthetic strategy based on the *O*-alkylation of the VHL ligand with a trifunctional PEG linker bearing a carboxylic acid for the macrolactamization and a protected amine for coupling to JQ1. The new stereocenter generated from the formal alkylation of the first ethylene glycol unit of MZ1 could be easily set by choosing the correct chiral glycerol equivalent. The synthesis of the trifunctional linker is detailed in Scheme 1 and started from commercially available (*S*)-(+)-1,2-isopropylideneglycerol **3** and 2-(2-

(benzyloxy)ethoxy)ethyl 4-methylbenzenesulfonate **4**. Alkylation was performed in solid-liquid phase transfer catalysis (S-L PTC) conditions using potassium hydroxide as a base and tetrabutylammonium iodide as catalyst and afforded compound **5** in 52% yield. The acetonide deprotected was achieved in aqueous acetic acid to obtain the diol **6** in quantitative yield. Selective primary alcohol protection with *tert*-butyl dimethyl silyl chloride afforded the TBS ether **7**, which underwent functional group interconversion via mesylate to obtain the azide **8**. Subsequent deprotection of the silyl ether and alkylation with mesylate **9** led to the trityl-protected compound **10** in excellent yield. Removal of the trityl group was achieved with diluted TFA and triisopropyl silane (10% in DCM) to afford alcohol **11**. Reaction with *tert*-butyl bromoacetate in PTC conditions led to ester **12** in 71% yield. Hydrogenative palladium-catalyzed debenzylation and azide reduction, followed by Alloc protection afforded the key trifunctional linker **13**.

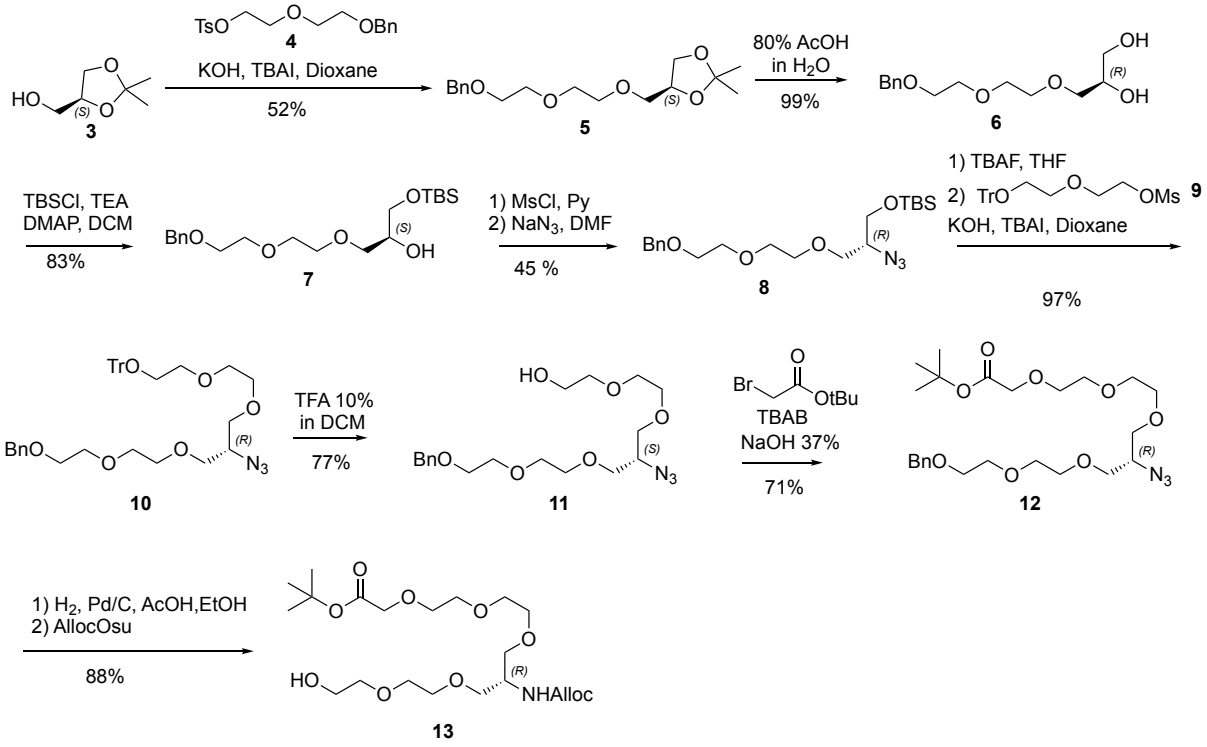

Scheme 1. Synthesis of trifunctional linker **13**.

With the trifunctional linker in hand, we next proceeded to alkylate the Boc-protected VHL ligand **15**. The mesylate **14** (obtained from **13** and mesyl chloride) was reacted with **15** and potassium carbonate in DMF to give compound **16** in 64% yield. The latter was treated with TFA to simultaneously deprotect the *tert*-butyl ester and the Boc protecting group. After

exchanging the trifluoroacetate counterion with hydrochloride by freeze drying from a diluted HCl solution, macrolactamization was performed with HATU in high dilution (1.7 mM in DCM) to afford compound **17** in 75% yield. Alloc deprotection was achieved with tetrakis(triphenylphosphine)palladium and an excess of phenylsilane. Finally, amide coupling with JQ1-COOH in the presence of COMU and DIPEA afforded compound **1** in 32% isolated yield from **17** (Scheme 2).

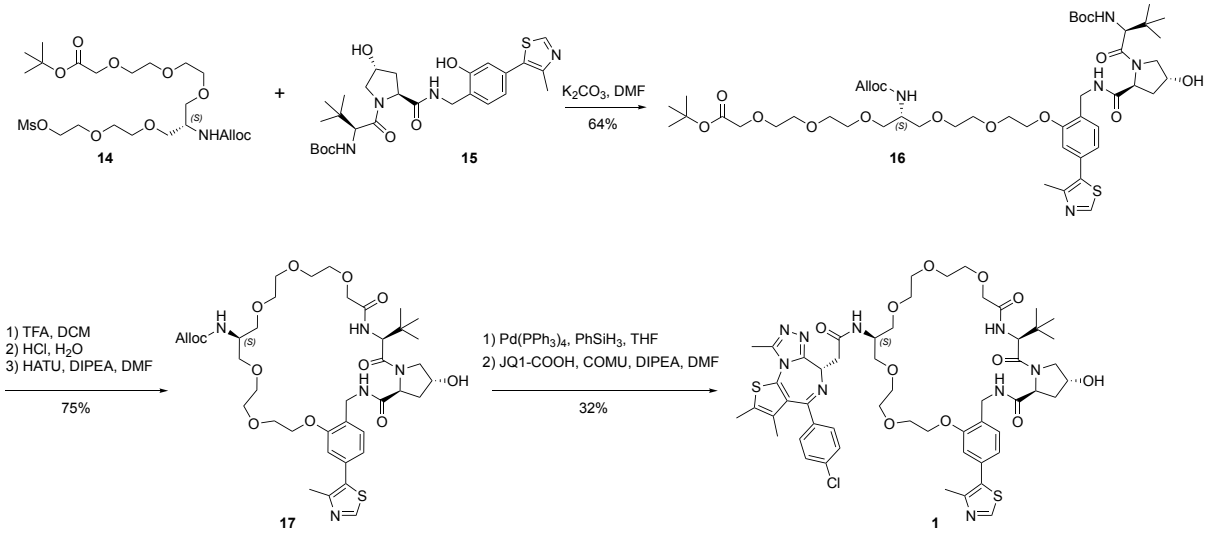

Scheme 2. Macrolactamization and completion of the synthesis of the macroPROTAC-1.

To assess the extent to which macrocyclization impacted on the formation of PROTAC ternary complexes between VHL and BET bromodomains, we next turned to biophysical ternary complex assays. First, we performed a competitive fluorescence polarization (FP) assay.[15] In this assay, a fluorescent HIF-1α peptide probe bound to VHL is displaced in a dose-response fashion by either PROTAC alone or PROTAC pre-incubated with individual BET bromodomains. Positive cooperativity (α) would result in a left-shift of the curve (higher binding affinity) in the presence of the bromodomain. Compound **1** (herein referred to as macroPROTAC-1) retained high binding affinity to VHL (K_i = 33 nM, Figure 2A). We observed cooperative formation of ternary complexes with the second bromodomain of Brd4, Brd2 and, to a lesser extent, Brd3 (α = 10.5, 9.5 and 4.0, respectively). In contrast, no cooperativity was observed with the first bromodomain of Brd3, Brd4 and Brd2 (α = 0.9, 0.8 and 0.7, respectively). This contrasts with MZ1, which could still form cooperative complexes with all the target bromodomains,[10,15] and suggests that macroPROTAC-1 better

differentiates the second bromodomains versus the first bromodomains of the BET proteins compared to MZ1.

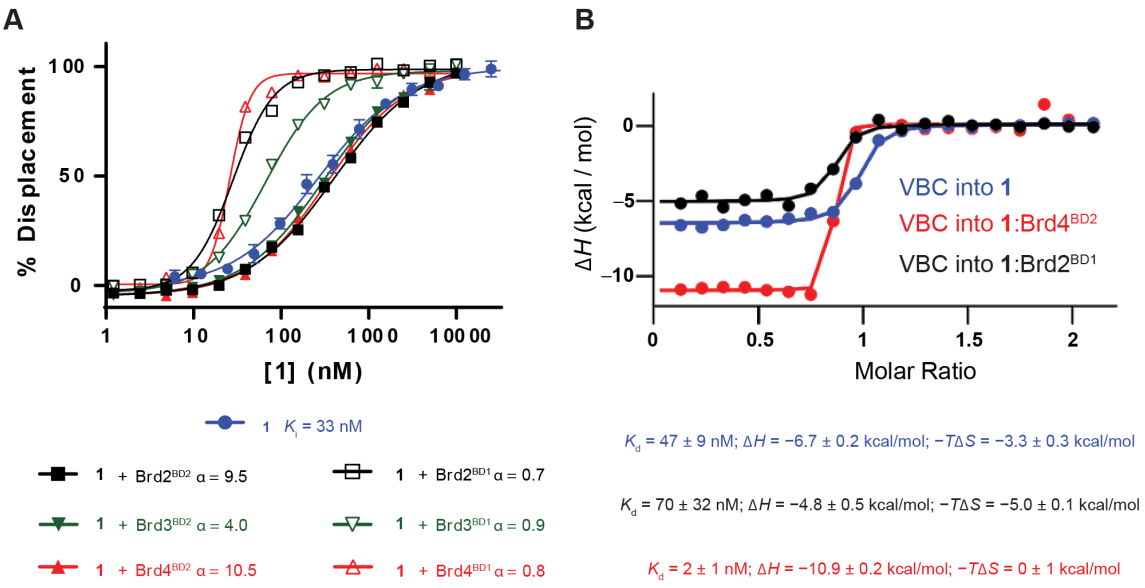

Figure 2. Binding and cooperativity of ternary complex formation. (A) Dose-dependent displacement of a fluorescent Hif1-α peptide by **1** alone or **1** in complex with a BET bromodomain, measured by fluorescence polarization. Cooperative binding is observed for all the BD2s while non cooperative or negatively cooperative binding is observed for the BD1s. (B) Representative inverse ITC titrations of VBC into **1** and VBC into **1**:Brd2^{BD1} or **1**:Brd4^{BD2} showing cooperative binding in the case of Brd4^{BD2} and negatively cooperative binding in the case of Brd2^{BD1}.

To gain more insights on the effect of cyclization on the thermodynamics of ternary complex formation, the binding affinity of macroPROTAC-1 for VHL and selected BET proteins was studied by ITC (Supplementary Figure S4). For these experiments, among the six BET proteins, we selected Brd2^{BD1} and Brd4^{BD2} as they formed the least cooperative and most cooperative ternary complex according to our FP data. MacroPROTAC-1 bound to VHL with K_d = 47 ± 9 nM and ΔH of –6.7 ± 0.2 kcal /mol (Figure 2B), comparably to MZ1 (K_d = 66 ± 6 nM and ΔH of –7.7 ± 0.3 kcal /mol)[10]. Interestingly, much weaker binary binding affinities were detected for the bromodomains (Brd4^{BD2} Kd = 180 nM, c.f. with 15 nM for MZ1; Brd2^{BD1} Kd = 740 nM, c.f. with 62 nM for MZ1, Table 1), corresponding to 12-fold loss of binary affinity compared to MZ1 in each case.[10] Thermodynamics of formation of ternary complexes VHL:**1**:Brd2^{BD1} and VHL:**1**:Brd4^{BD2} revealed high positive cooperativity of VHL-Brd4^{BD2} (α = 20, c.f. with 17.6 for MZ1) and a negatively cooperative complex with VHL-

$Brd2^{BD1}$ (α = 0.7, c.f. with 2.9 for MZ1, Figure 2B and Table 1). Together, the biophysical data is consistent with a better discrimination between the highly homologous BET bromodomains when using macroPROTAC-1 compared to its non-cyclic progenitor.

Table 1: Thermodynamic parameters of formation of binary and ternary complexes between **1** and MZ1, VHL-ElonginB-ElonginC (VBC), $Brd2^{BD1}$ and $Brd4^{BD2}$. The reported values are the mean ± standard deviation from independent measurements. For titrations of MZ1, the data is taken from [10].

Protein in syringe	Species in cell	K_d (nM)	ΔH (kcal mol^{-1})	ΔG (kcal mol^{-1})	$-T\Delta S$ (kcal mol^{-1})	α	Total ΔG (kcal mol^{-1})	No. of replicate
$Brd2^{BD1}$	**1**	743 ± 202	–9.6 ± 0.6	–8.4 ± 0.2	1.2 ± 0.7	-	-	2
$Brd4^{BD2}$	**1**	180 ± 42	–6.25 ± 0.17	–9.2 ± 0.2	–2.7 ± 0.3	-	-	2
VBC	**1**	47 ± 9	–6.7 ± 0.2	–10.0 ± 0.1	–3.3 ± 0.3	-	-	3
VBC	**1**: $Brd2^{BD1}$	70 ± 32	–4.8 ± 0.5	–9.9 ± 0.4	–5.0 ± 0.1	0.7	–18.3 ± 0.4	2
VBC	**1**: $Brd4^{BD2}$	2 ± 1	–10.9 ± 0.2	–11.9 ± 0.3	–1.0 ± 0.4	20	–21.1 ± 0.4	2
$Brd2^{BD1}$	MZ1	62 ± 6	–12.8 ± 0.7	–9.84 ± 0.06	3.0 ± 0.8	-	-	2
$Brd4^{BD2}$	MZ1	15± 1	–10.9 ± 0.4	–10.68 ± 0.04	0.2 ± 0.4	-	-	2
VBC	MZ1	66 ± 6	–7.7 ± 0.3	–9.81 ± 0.05	–2.1 ± 0.3	-	-	8
VBC	MZ1: $Brd2^{BD1}$	24 ± 8	–7.3 ± 0.2	–10.4 ± 0.2	–3.1 ± 0.4	2.9	–20.3 ± 0.2	2
VBC	MZ1: $Brd4^{BD2}$	3.7 ± 0.7	–8.9 ± 0.1	–11.5 ± 0.1	–2.6 ± 0.2	17.6	–22.2 ± 0.2	2

To validate the binding mode and deepen understanding of the molecular basis for the biophysical properties of macroPROTAC-1, we next co-crystallised VHL:macroPROTAC-1:$Brd4^{BD2}$ and solved the structure of the ternary complex at a resolution of 3.5 Å (Figure 3 and supplementary figure S5). The structure superposes well with the ternary complex VHL:MZ1:$Brd4^{BD2}$ (C-alpha RMSD = 0.593 Å) and recapitulates the major PPIs between VHL and $Brd4^{BD2}$. Conserved contacts include the previously reported electrostatic interactions between $Arg107^{VHL}$, $Arg108^{VHL}$, $D381^{Brd4}$ and $E383^{Brd4}$; and the stack between the canonical WPF shelf of Brd4 and Pro71 of VHL (Figure 3A). Collectively, these interactions result in a buried surface area (BSA) between the two proteins of 681 $Å^2$. The MZ1-portion of macroPROTAC-1 binds in an identical S-shaped conformation as the uncyclized PROTAC, retaining the H-bond between His437 and an oxygen atom on the PEG-3 linker. The cyclizing part of the linker optimally fills an additional cavity created at the interface of the two proteins next to the ZA-loop (Figure 3A and supplementary figure S6), which is in good agreement with the MD simulations (Figure 1D and supplementary figure S2). The BSA at the

macroPROTAC-1:VHL and macroPROTAC-1:Brd4^{BD2} interfaces are 961 and 1064 Å^2, respectively, which brings the total BSA to 2686 Å^2. Taken together, these findings could explain the high cooperativity of VHL: macroPROTAC-1:Brd4^{BD2}. Closer examination of the additional linker revealed potential clashes with the ZA-loop, which could explain the loss in binding affinity with the BET bromodomains. Within the ZA-loop, the side chain of Leu387, as well as the carbonyl oxygens of both Gly386 and Leu385, are less than 3.5 Å from the newly added linker. Interestingly, the clash with Leu387 is similar to that exploited in our bump-and-hole study for the same residue (Figure 3B).[29,30] The enhanced discrimination between BD1 and BD2 could potentially be attributed to differences in the ZA-loop of BD1s compared to BD2s. Sequence alignment of the six bromodomains revealed an additional proline (Pro397) in BD1 which could limit the ability of the BD1s to accommodate the extra linker present in macroPROTAC-1 (supplementary figure S7).

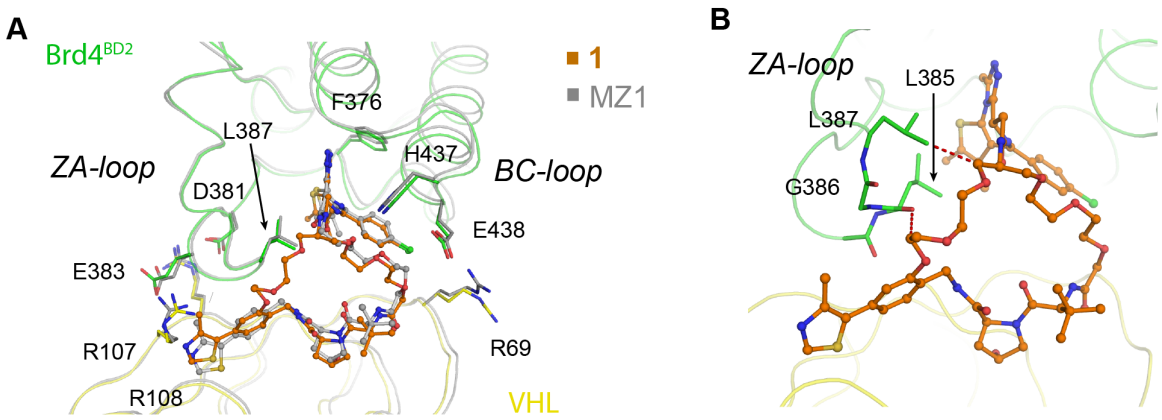

Figure 3. Crystal structure of ternary complex VHL:**1**:Brd4^{BD2}. (A) Superposition of VHL:**1**:Brd4^{BD2} (green and yellow) and VHL:MZ1:Brd4^{BD2} ternary complex (PDB 5T35; grey) highlighting the key protein-protein interactions between VHL and Brd4^{BD2}. (B) Residues in the ZA-loop of Brd4^{BD2} (Leu385, Gly386 and Leu287) that are in close proximity to the additional linker on **1**. Red dashes indicate atom pairs that are ≤ 3.5 Å apart.

We next investigated the cellular activities of macroPROTAC-1. First, HeLa cells were treated with macroPROTAC-1 or MZ1 for 4 h or 18 h before cell lysis and Western blotting (supplementary figure S8). MacroPROTAC-1, like MZ1, was able to induce potent and rapid degradation of Brd4 (both short and long isoforms) with a DC_{50} between 25 and 125 nM, while degradation of Brd2 and Brd3 occurred only at higher concentrations, with a DC_{50} > 125 nM. Degradation of the BET protein and downstream effects on Myc levels after

treatment with macroPROTAC-1 or MZ1 were next assessed in a disease-relevant cell line, 22RV1 (human prostate carcinoma, Figure 4A-B). MacroPROTAC-1 induced > 90% depletion of Brd4 at 250 nM. MacroPROTAC-1 also induced >90 % depletion of cellular levels of Myc in 22RV1 cells, as downstream effect of BET degradation, with potency and kinetics comparable to MZ1 (Figure 4A-B).

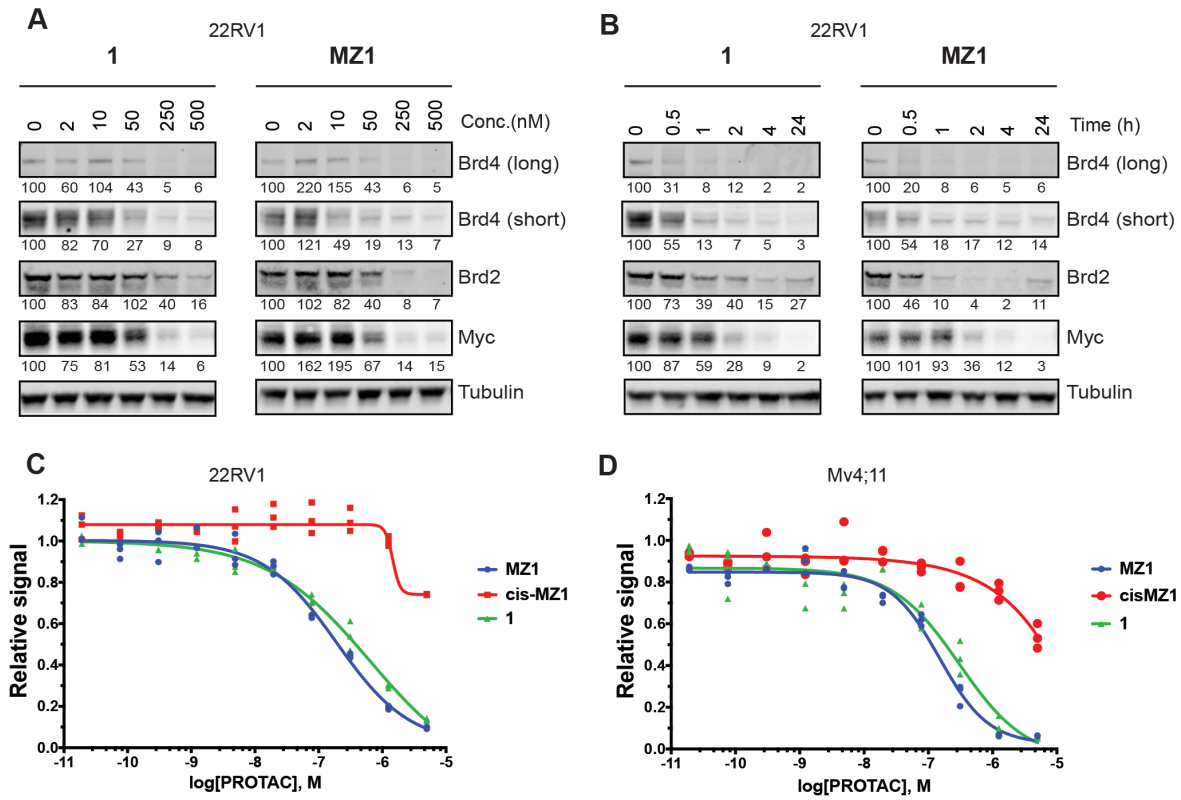

Figure 4. Cellular activity of macroPROTAC-1. (A) 22RV1 cells were treated with different concentrations of **1** or MZ1 for 4 h. (B) 22RV1 cells were treated with 500 nM of **1** or MZ1 for different times. In A and B, protein levels were analyzed by Western blotting using corresponding antibodies after SDS-PAGE. (C-D) Antiproliferative activity of **1**, MZ1 and cisMZ1. 22RV1 (C) and MV4;11 (D) cells were treated with compounds for 72 and 48 h respectively prior to quantitation of cell proliferation using the CellTiter-Glo luminescent cell viability assay.

We next evaluated the impact of compound **1** on the viability of BET-sensitive human prostate carcinoma 22RV1 and acute myeloid leukemia MV4;11 cancer cell lines (Figure 4 C-D). MacroPROTAC-1 induced a marked antiproliferative effect with an EC_{50} of 640 nM in 22RV1 cells (Figure 5A) and an EC_{50} of 300 nM in MV4;11 cells (Figure 5B), a potency comparable to MZ1. Compound *cis*MZ1, which does not induce BET degradation but can still inhibit the BET proteins, was used as a reference control to confirm that cytotoxicity is due to BET degradation and not inhibition.[7] Taken together, these results show that

macroPROTAC-1 has a very similar cellular activity to MZ1, despite its 12-fold weaker binary binding affinity at the bromodomain end.

In conclusion, this work illustrates a successful roadmap to macrocyclization PROTAC design strategies. Macrocyclization allows the constraint of a PROTAC molecule in its bioactive conformation, biasing it to adopt or discriminate against a desired ternary complex, which we show can aid degradation potency and selectivity amongst homologous targets. Our work also highlights that the binary binding energies of the PROTAC for the target protein (and E3 ligase) should ideally not be detrimentally impacted as a result of the cyclization process, and we suggest this to be monitored closely in future applications. We anticipate that structure-based design of macrocyclic PROTACs will be an increasingly attractive and feasible strategy of PROTAC design, in particular as relevant structural information continues to emerge and impact the field.

Acknowledgements

This project has received funding from the European Research Council (ERC) under the European Union's Seventh Framework Programme (FP7/2007−2013) as a Starting Grant to A.C. (grant agreement no. ERC-2012-StG-311460 DrugE3CRLs). X.L. was supported by a Marie Skłodowska-Curie Actions Individual Fellowship from the European Commission (H2020-MSCA-IF-2015-806323). Biophysics and drug discovery activities were supported by Wellcome Trust strategic awards to Dundee (100476/Z/12/Z and 094090/Z/10/Z, respectively).

Data availability: Atomic coordinates and structure factors for the crystal structure VCB:**1**:Brd4^{BD2} have been deposited in the PDB under accession number 6SIS.

Notes: The Ciulli laboratory receives or has received sponsored research support from Boehringer Ingelheim, Eisai Inc., Nurix Inc., and Ono Pharma. A.C. is a scientific founder, director and shareholder of Amphista Therapeutics, a company that is developing targeted protein degradation therapeutic platforms.

References

[1] P. M. Cromm, C. M. Crews, *Cell Chem Biol* **2017**, *24*, 1181–1190.
[2] R. Chopra, A. Sadok, I. Collins, *Drug Discovery Today: Technologies* **2019**, *31*, 5–13.
[3] S. J. Hughes, A. Ciulli, *Essays Biochem* **2017**, *61*, 505–516.
[4] I. Churcher, *J. Med. Chem.* **2018**, *61*, 444–452.
[5] M. Pettersson, C. M. Crews, *Drug Discovery Today: Technologies* **2019**, *31*, 15–27.
[6] G. E. Winter, D. L. Buckley, J. Paulk, J. M. Roberts, A. Souza, S. Dhe-Paganon, J. E. Bradner, *Science* **2015**, *348*, 1376–1381.
[7] M. Zengerle, K.-H. Chan, A. Ciulli, *ACS Chem Biol* **2015**, *10*, 1770–1777.
[8] J. Lu, Y. Qian, M. Altieri, H. Dong, J. Wang, K. Raina, J. Hines, J. D. Winkler, A. P. Crew, K. Coleman, et al., *Chem Biol* **2015**, *22*, 755–763.
[9] D. P. Bondeson, A. Mares, I. E. D. Smith, E. Ko, S. Campos, A. H. Miah, K. E. Mulholland, N. Routly, D. L. Buckley, J. L. Gustafson, et al., *Nat Chem Biol* **2015**, *11*, 611–617.
[10] M. S. Gadd, A. Testa, X. Lucas, K.-H. Chan, W. Chen, D. J. Lamont, M. Zengerle, A. Ciulli, *Nat Chem Biol* **2017**, *13*, 514–521.
[11] C. Maniaci, A. Ciulli, *Curr Opin Chem Biol* **2019**, *52*, 145–156.
[12] A. Zorba, C. Nguyen, Y. Xu, J. Starr, K. Borzilleri, J. Smith, H. Zhu, K. A. Farley, W. D. Ding, J. Schiemer, et al., *P Natl Acad Sci Usa* **2018**, *115*, E7285–E7292.
[13] R. P. Nowak, S. L. DeAngelo, D. Buckley, Z. He, K. A. Donovan, J. An, N. Safaee, M. P. Jedrychowski, C. M. Ponthier, M. Ishoey, et al., *Nat Chem Biol* **2018**, *14*, 706–714.
[14] S. L. Fisher, A. J. Phillips, *Curr Opin Chem Biol* **2018**, *44*, 47–55.
[15] M. J. Roy, S. Winkler, S. J. Hughes, C. Whitworth, M. Galant, W. Farnaby, K. Rumpel, A. Ciulli, *ACS Chem Biol* **2019**, *14*, 361–368.
[16] K. M. Riching, S. Mahan, C. R. Corona, M. McDougall, J. D. Vasta, M. B. Robers, M. Urh, D. L. Daniels, *ACS Chem Biol* **2018**, *13*, 2758–2770.
[17] D. P. Bondeson, B. E. Smith, G. M. Burslem, A. D. Buhimschi, J. Hines, S. Jaime-Figueroa, J. Wang, B. D. Hamman, A. Ishchenko, C. M. Crews, *Cell Chem Biol* **2018**, *25*, 78–87.e5.
[18] B. Jiang, E. S. Wang, K. A. Donovan, Y. Liang, E. S. Fischer, T. Zhang, N. S. Gray, *Angew Chem Int Ed Engl* **2019**, *58*, 6321–6326.
[19] R. L. M. van Montfort, P. Workman, *Essays Biochem* **2017**, *61*, 431–437.
[20] W. Farnaby, M. Koegl, M. J. Roy, C. Whitworth, E. Diers, N. Trainor, D. Zollman, S. Steurer, J. Karolyi-Oezguer, C. Riedmueller, et al., *Nat Chem Biol* **2019**, *15*, 672–680.
[21] E. A. Villar, D. Beglov, S. Chennamadhavuni, J. A. Porco, D. Kozakov, S. Vajda, A. Whitty, *Nat Chem Biol* **2014**, *10*, 723–731.
[22] A. Glas, E. C. Wamhoff, D. M. Krüger, C. Rademacher, T. N. Grossmann, *Chemistry* **2017**, *23*, 16157–16161.
[23] T. A. F. Cardote, A. Ciulli, *ChemMedChem* **2016**, *11*, 787–794.
[24] E. Valeur, S. M. Guéret, H. Adihou, R. Gopalakrishnan, M. Lemurell, H. Waldmann, T. N. Grossmann, A. T. Plowright, *Angew Chem Int Ed Engl* **2017**, *56*, 10294–10323.
[25] S. Alihodžić, M. Bukvić, I. J. Elenkov, A. Hutinec, S. Koštrun, D. Pešić, G. Saxty, L. Tomašković, D. Žiher, *Prog Med Chem* **2018**, *57*, 113–233.
[26] D. Benjamin, M. Colombi, C. Moroni, M. N. Hall, *Nat Rev Drug Discov* **2011**, *10*, 868–880.

[27] S. A. Andrei, E. Sijbesma, M. Hann, J. Davis, G. O'Mahony, M. W. D. Perry, A. Karawajczyk, J. Eickhoff, L. Brunsveld, R. G. Doveston, et al., *Expert Opin.Drug Discov.* **2017**, *12*, 925–940.
[28] M. Avalos, R. Babiano, J. L. Barneto, J. L. Bravo, P. Cintas, J. L. Jiménez, J. C. Palacios, *J Org Chem* **2001**, *66*, 7275–7282.
[29] M. G. J. Baud, E. Lin-Shiao, T. Cardote, C. Tallant, A. Pschibul, K.-H. Chan, M. Zengerle, J. R. Garcia, T. T. L. Kwan, F. M. Ferguson, et al., *Science* **2014**, *346*, 638–641.
[30] A. C. Runcie, M. Zengerle, K. H. Chan, A. Testa, L. Van Beurden, M. G. J. Baud, O. Epemolu, L. C. J. Ellis, K. D. Read, V. Coulthard, et al., *Chem Sci* **2018**, *9*, 2452–2468.

Structure-Based Design of a Macrocyclic PROTAC

Andrea Testa, Scott J. Hughes, Xavier Lucas, Jane E. Wright, Alessio Ciulli*

Division of Biological Chemistry and Drug Discovery, School of Life Sciences, University of Dundee, Dow Street, Dundee, DD1 5EH, Scotland, United Kingdom

Table of Contents

Supplementary Figures ***2***

Computational methods ***9***

Chemistry ***11***

Protein expression and purification ***22***

Isothermal titration calorimetry (ITC) ***22***

Fluorescence polarization assay ***24***

Crystallography ***24***

Tissue culture ***27***

Testing compounds in cells ***27***

Immunoblotting ***27***

Cell Viability Assay ***28***

Copies of NMR spectra ***29***

Supplementary Figures

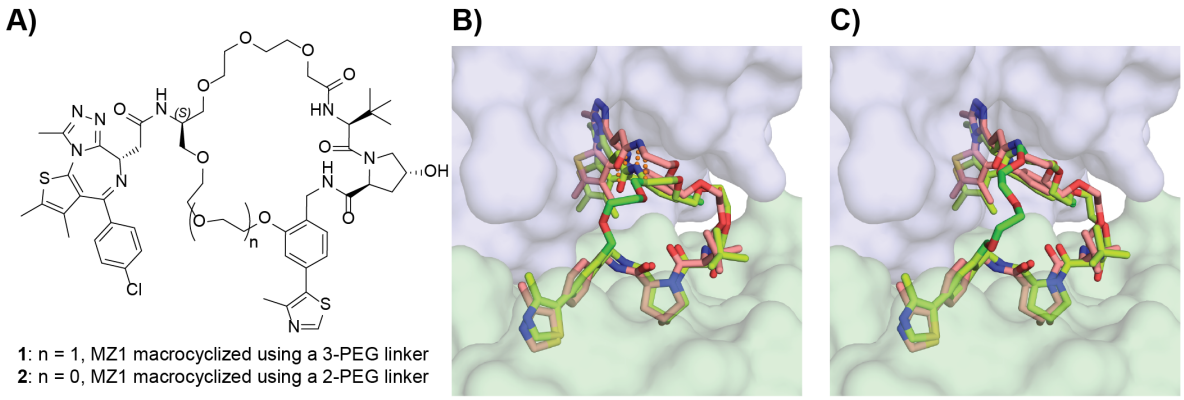

Figure S1. Structure and modeling of macrocyclic MZ1 derivatives. *(A) Chemical structures of cyclized derivatives **1** and **2**. (B, C) Superposition of the crystallographic pose of MZ1 (in salmon) and the energy-minimized structure of macrocyclic derivatives with a linker comprising (B) 2 PEG units and (C) 3 PEG units (in lime, with the new PEG linkers colored green). The surface of VHL and Brd4^{BD2} is colored pale green and light blue, respectively. In (B), atomic displacements > 1.5 Å upon energy-minimization are highlighted in dotted orange lines. No such large rearrangements were observed in (C), suggesting that the linker was more appropriate.*

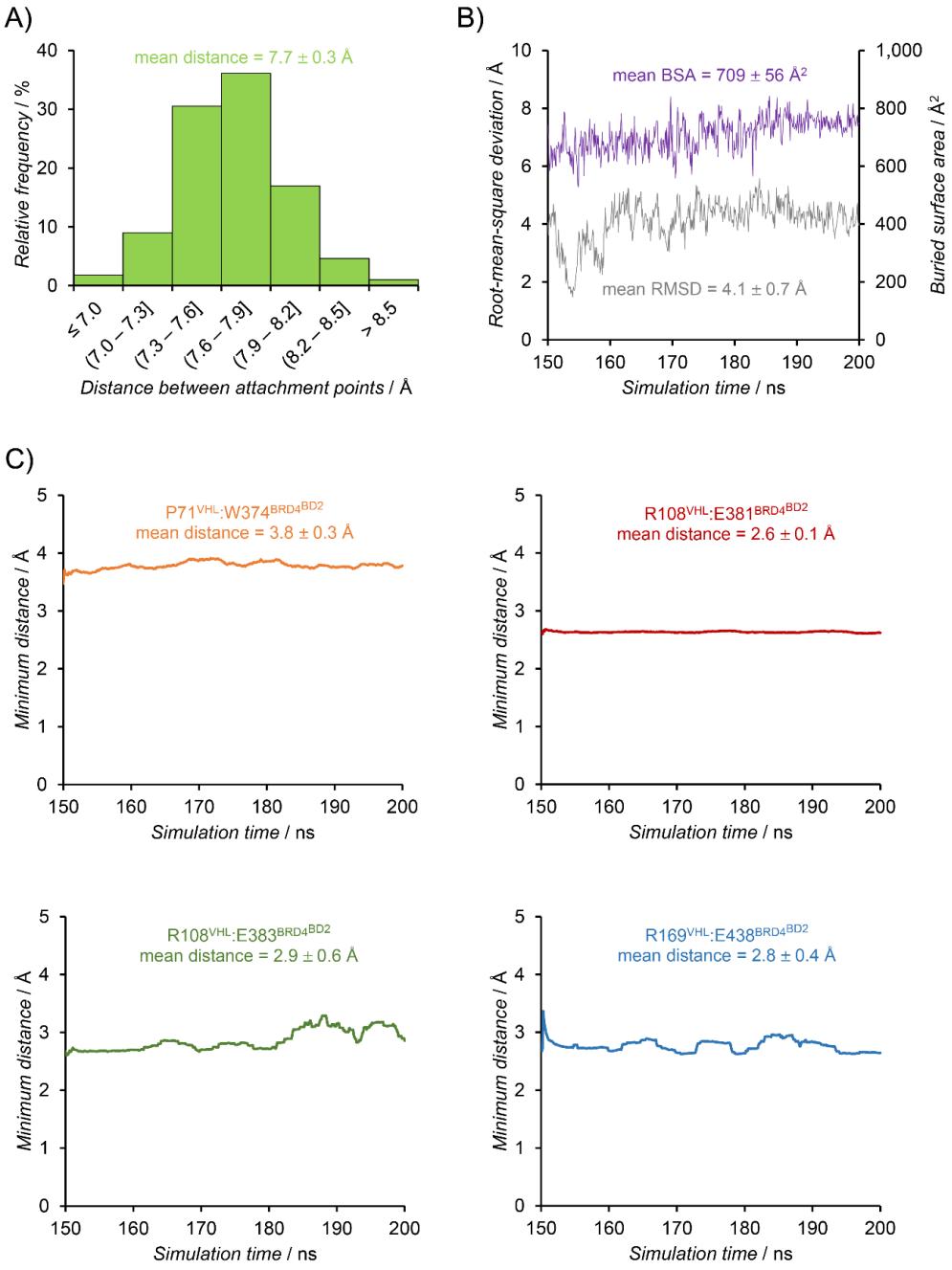

Figure S2. Structural integrity and stability of the VHL:1:Brd4^{BD2} ternary complex along the MD simulation. *(A) Histogram depicting the observed relative frequency of binned distances between the attachment points in compound* ***1****. (B) Buried surface area (BSA) in the interface of VHL with Brd4^{BD2} and root-mean-square deviation (RMSD) of all α-carbon atoms in the proteins, after superposition to the crystal structure of VCB:MZ1:Brd4^{BD2} (PDB code 5T35).[1] (C) Minimum distance between selected amino acids in VHL and Brd4^{BD2} that participate in protein–protein interactions.[1] For clarity, the plotted distances are the average over 5 ns. In all cases, only the last 50 ns in 100 ps intervals of a 200-ns MD simulation of the VHL:**1**:Brd4^{BD2} ternary complex were considered to generate the data. The mean ± 1 s.d. of each measurement is shown.*

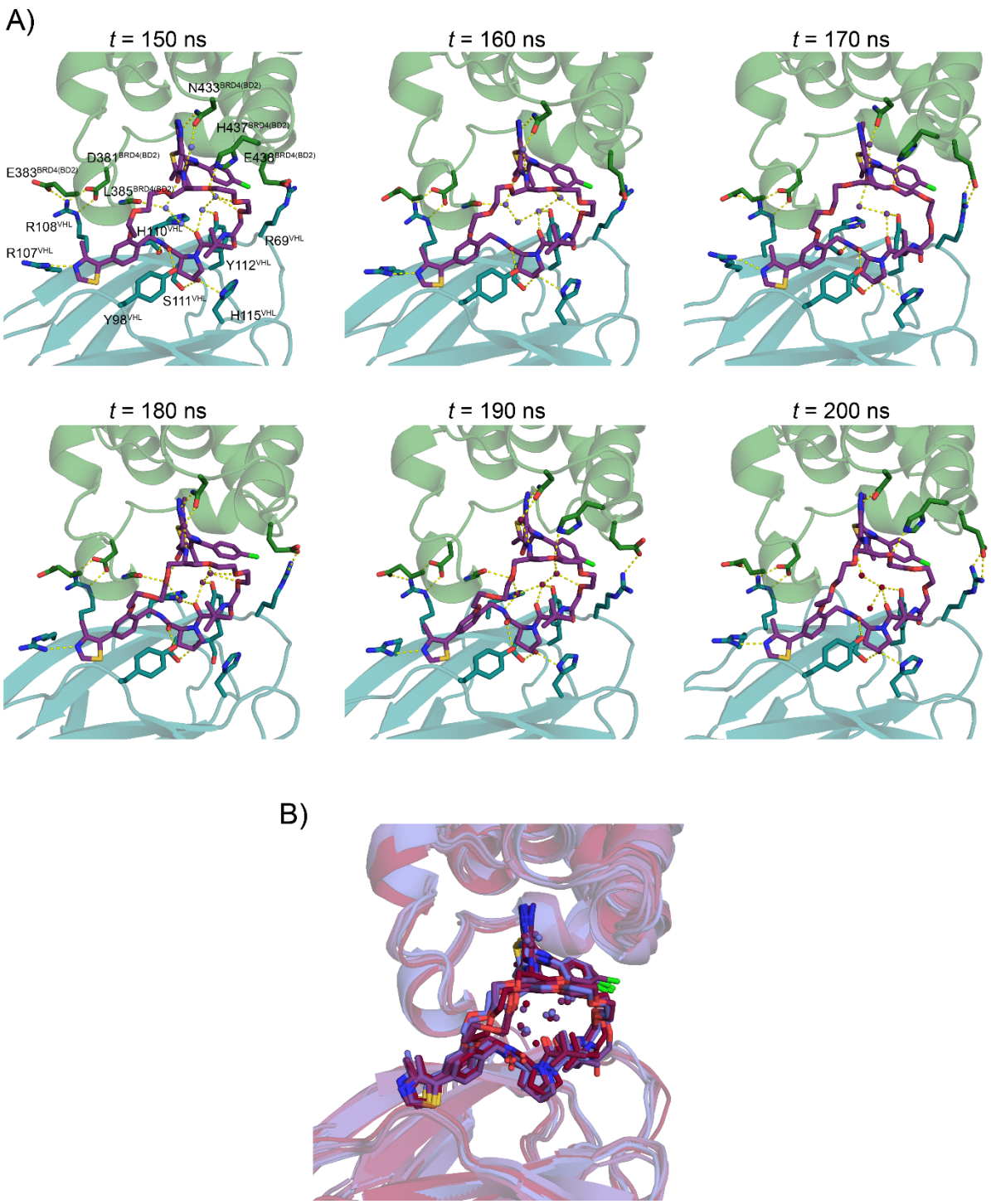

Figure S3. Interactions in the VHL:1:Brd4^{BD2} ternary complex along the MD simulation. *(A) Protein–protein and protein–ligand interactions (showed in dashed yellow lines) observed at 10 ns intervals along the last 50 ns of a 200-ns MD simulation of the VHL:**1**:Brd4^{BD2} ternary complex. A conserved water network stabilized at the interface of the three partners is shown along the simulation. In the first panel, interacting amino acids in VHL and Brd4^{BD2} are labelled. (B) Superposition of the frames showed in (A), with the time lapse colored from blue to dark red. Water molecules within the network form clusters at specific locations of the interface, indicating that they engage in stabilizing interactions with their surrounding during the simulation.*

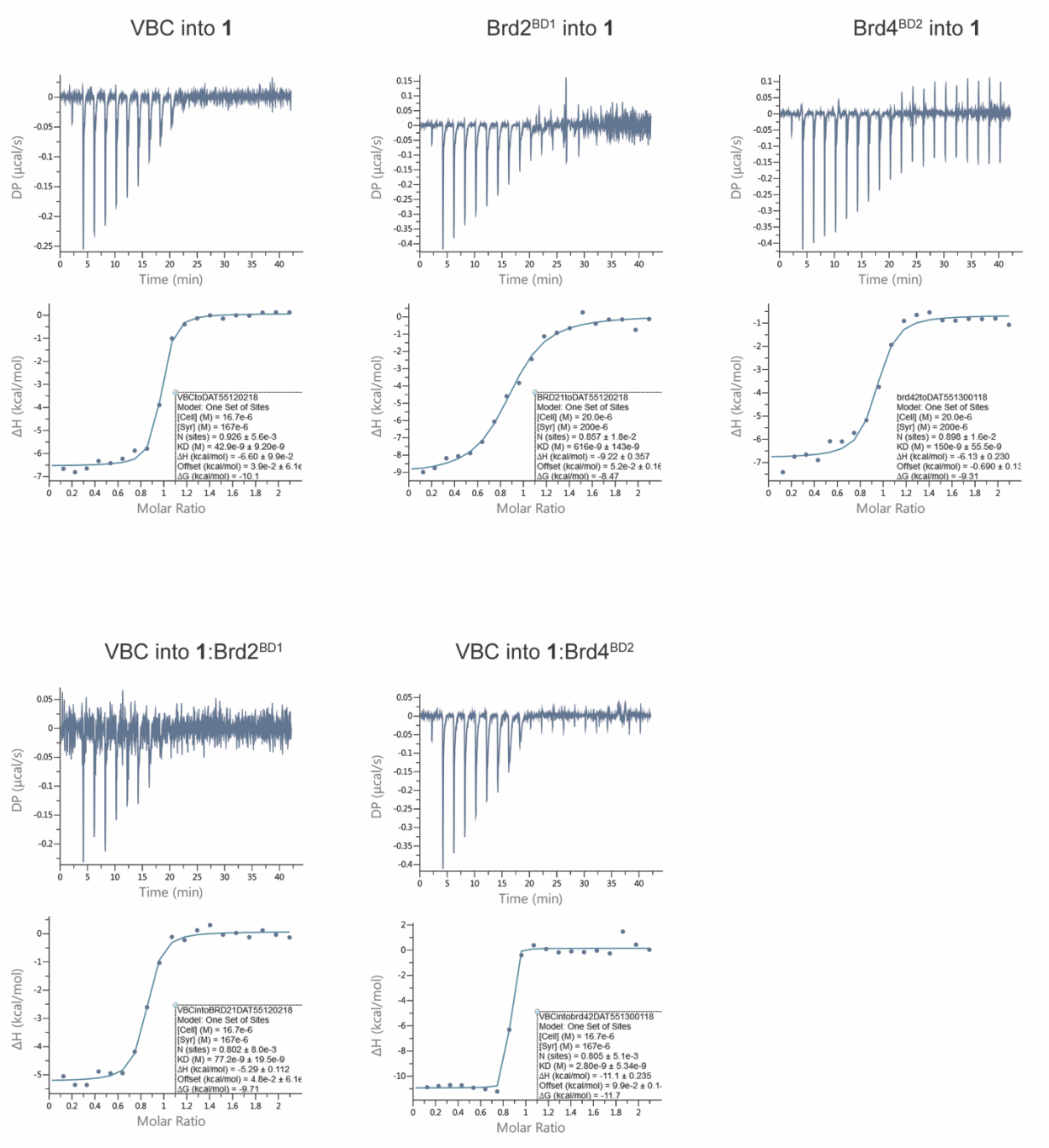

Figure S4. *Representative ITC titrations obtained for compound 1 and VBC,Brd2^{BD1} and Brd4^{BD2}.*

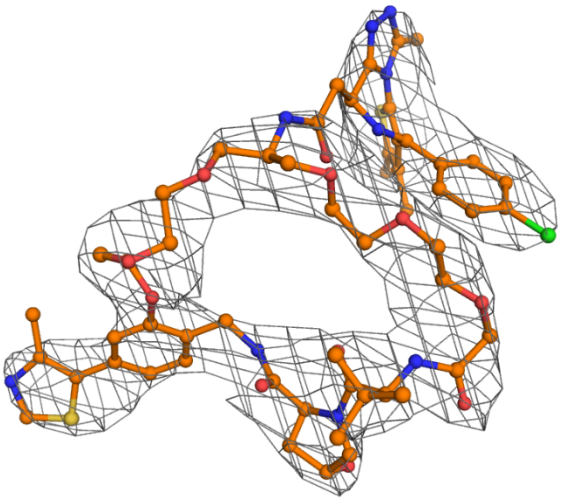

***Figure S5**. Fo – Fc omit map of compound **1** (contoured at 2.8 σ; carve = 2) showing electron density for the additional linker*

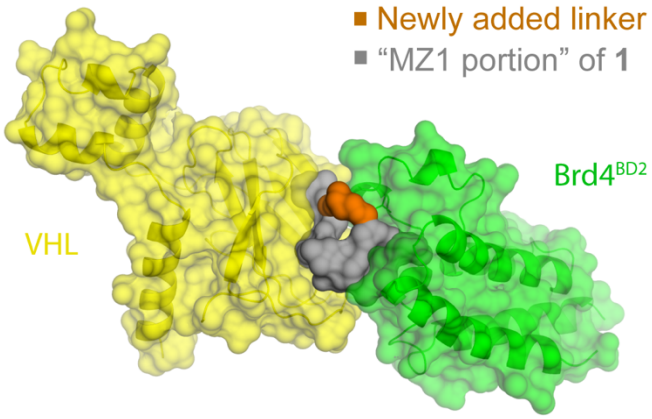

***Figure S6**. Surface representation of VCB:**1**:Brd4^{BD2} ternary complex highlighting cavity filled by the "MZ1-portion"(gray) and additional linker (orange) of compound **1**.*

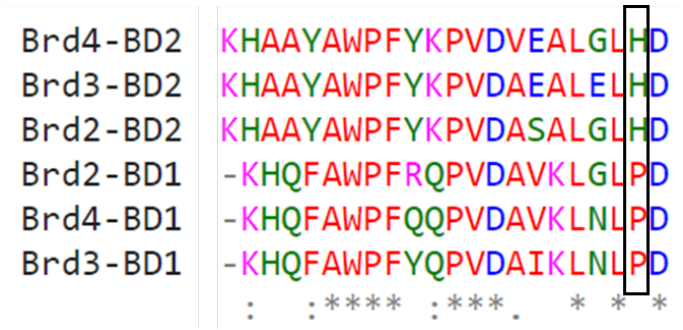

***Figure S7** Sequence alignment of ZA-loop from the bromodomains of Brd2, Brd3 and Brd4 highlighting the presence of an additional proline in the* ZA-loop of *BD1s.*

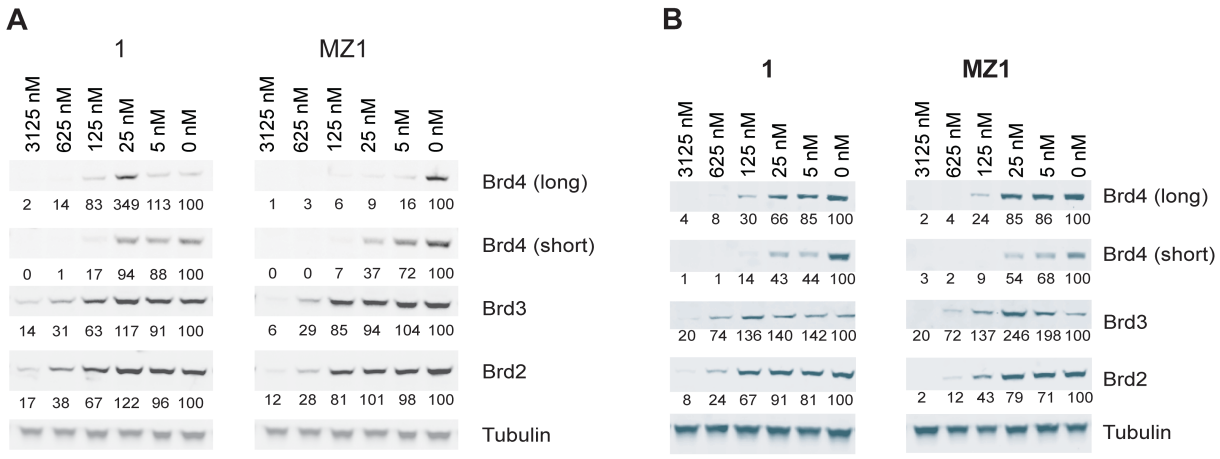

Figure S8. *(A-B) Protein levels in HeLa cells after treatment with compound 1 or MZ1 for 18h (A) or 4h (B) visualised and quantified by Western blot.*

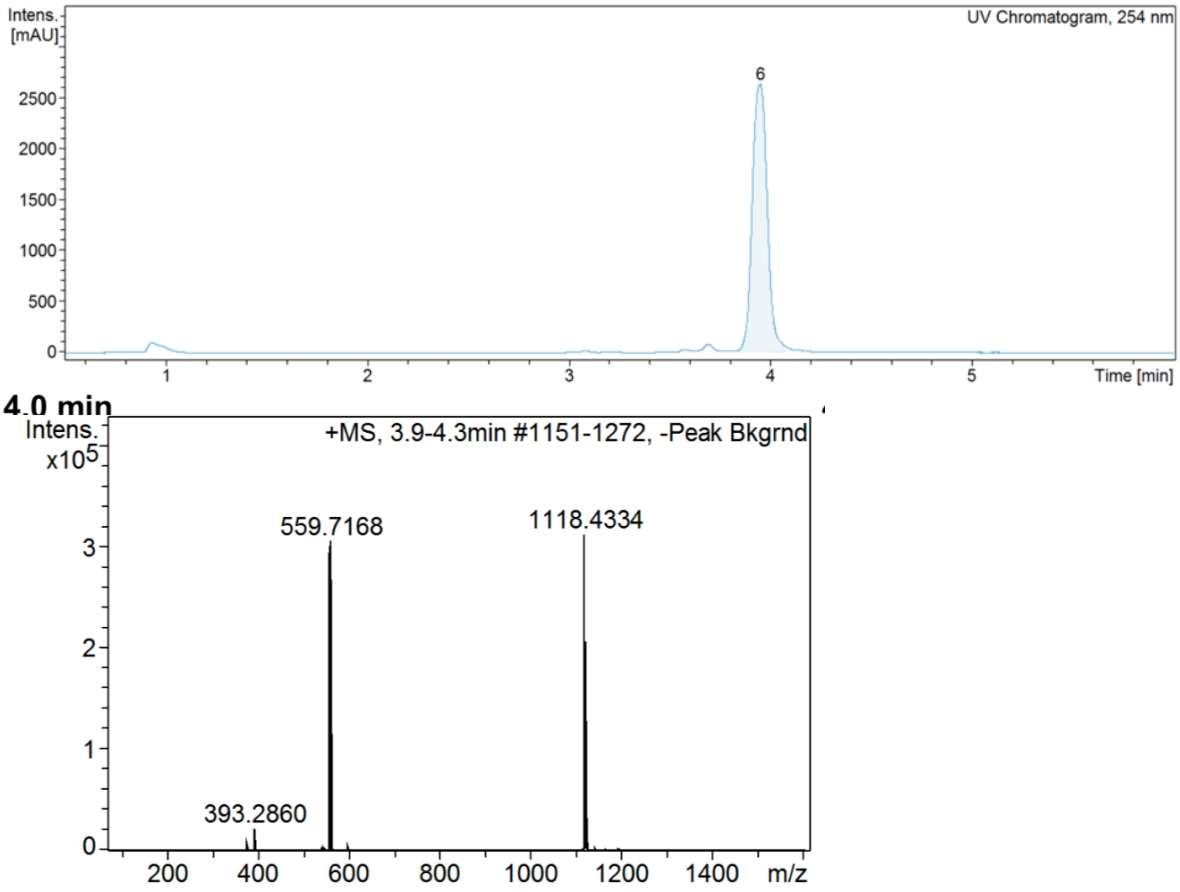

Figure S5**. Analytical HPLC trace (254 nm) and HRMS of purified compound **1

Computational methods

Torsion analysis of surrogate N-substituted acetamides

Model compounds *N*-ethylacetamide and *N*-isopropylacetamide (Fig. 1C) were subjected to a relaxed torsion scan analysis of their alkylacetamide bond using density functional theory (DFT) at the PBF (water) MN15-L/aug-cc-pVTZ(-F) level of theory in Jaguar 9.7 (Schrödinger, LLC). The *C–N–C–C* torsion was gradually rotated from 0 to 180º in 10º steps, considering Abelian molecular symmetry when appropriate.

Molecular modeling of macrocyclic MZ1 derivatives

Derivatives of MZ1 macrocyclized using a 2-PEG and a 3-PEG linker (Fig. 1D) were modeled *in situ* using the VHL:MZ1:Brd4^{BD2} ternary complex crystal structure as template and Glide Ligand Designer (Schrödinger). Water and solvent molecules present in the protein crystal structure were removed, and the VHL:MZ1:Brd4^{BD2} system was prepared for energy minimization in Prime (Schrödinger) using the Protein Preparation Wizard (Schrödinger). Amino acid protonation states were assigned using PROPKA 3.0.[2]

*Molecular dynamics (MD) simulation of the VHL:**1**:Brd4^{BD2} ternary complex*

The energy-minimized model of VHL:**1**:Brd4^{BD2} was used as starting point for a molecular dynamics (MD) simulation. MD simulations were carried out in an nVIDIA TITAN X GPU using Desmond (Schrödinger) and the OPLS3 force field.[3] System Builder (Schrödinger) was used to solvate the complex in a TIP3P water box with a padding of 10 Å from the edge of the box to any solute atom, and to neutralize the system charges with three chloride ions. The solvated system was minimized for 2,000 steps with all protein and PROTAC atoms restrained to eliminate residual unfavorable interactions between the solute and the solvent, followed by another 2,000 steps with unrestrained PROTAC and solvent atoms, and lastly followed by another 5,000 steps with all atoms free to move. The equilibration phase consisted of an initial 100-ps Brownian dynamics simulation at 10 K with restraints on solute heavy atoms in the NVT ensemble, followed by one run of 120 ps of MD at the same temperature, restraints, and ensemble. The restrained system was

then subjected to two runs of 120 ps in the NPT ensemble, first at 10 K and then at 300 K, and a final unrestrained simulation at the final temperature (300 K) for 240 ps. We run 200 ns of MD (time step of 2 fs using the RESPA integrator), starting from the equilibrated system. The temperature was controlled with a Nose-Hoover chain thermostat at 300 K, and the pressure with a Martyna-Tobias-Klein barostat at 1 bar. Short-range nonbonded interactions were cut off at 9 Å. Only the last 50 ns of production simulation were used for data collection and analysis.

Analysis of MD trajectories

The last 50 ns of the 200-ns MD trajectory were analyzed using the Simulation Quality, Event, and Interactions Analysis tools, as included in Schrödinger. The buried surface area (BSA) of the proteins upon complex formation, *i.e.* the difference in surface-accessible surface area (SASA) between the formed complex and the unbound partners in each system, was computed using VMD v. 1.9.2 [4] and considering all protein atoms and a spherical probe of radius 1.4 Å.

System	*Number of atoms*	*Total energy* / Mcal mol^{-1}	*Pressure* / bar	*Volume* / nm^3	*Temperature* / K
VHL:1:$Brd4^{BD2}$	131,674	–335.6 ± 0.1	1 ± 65	1,328 ± 2	298.7 ± 0.8

Table S 1. Stability of the MD simulation of VHL:1:$Brd4^{BD2}$. *Number of atoms and physical properties of the system under simulation during the last 50 ns of a 200-ns MD simulation. Values given are the mean ± 1 s.d.*

Chemistry

All chemicals, unless otherwise stated were commercially available and used without further purification. Solvents were anhydrous and reactions preformed under positive pressure of nitrogen or argon. Enantiopure (+)-JQ-1 was purchased from Medchemexpress LLC, Princeton, USA. Flash column chromatography (FCC) was performed using a Teledyne Isco Combiflash Rf or Rf200i. As prepacked columns RediSep Rf Normal Phase Disposable Columns were used.

NMR spectra were recorded on a Bruker 500 Ultrashield or a Bruker Ascend 400. Chemical shifts are quoted in ppm and referenced to the residual solvent signals: ^{1}H $\delta = 7.26$ ($CDCl_3$), ^{13}C $\delta = 77.0$ ($CDCl_3$), ^{1}H $\delta = 3.32$ (MeOD), ^{13}C $\delta = 49.15$ (MeOD), ^{1}H $\delta = 2.50$ (DMSO-D6), ^{13}C $\delta = 39.51$(DMSO-D6). Signal splitting patterns are described as singlet (s), doublet (d), triplet (t), quartet (q), multiplet (m), broad (br) or a combination thereof. Coupling constants (*J*) are measured in Hz. Low resolution MS and analytical HPLC traces were recorded on an Agilent Technologies 1200 series HPLC connected to an Agilent Technologies 6130 quadrupole LC/MS, connected to an Agilent diode array detector. The column used was a Waters XBridge column (50 mm × 2.1 mm, 3.5 μm particle size) and the compounds were eluted with a gradient of 5−95% acetonitrile/water + 0.1% formic acid over 3 minutes (METHOD 1) or over 7 minutes (METHOD 2). Preparative HPLC was performed on a Gilson Preparative HPLC System with a Waters X-Bridge C18 column (100 mm x 19 mm; 5 μm particle size).

Abbreviations used: ACN for acetonitrile, COMU for (1-cyano-2-ethoxy-2-oxoethylidenaminooxy)dimethylamino-morpholino-carbenium hexafluorophosphate, DCM for dichloromethane, EtOAc for ethyl acetate, DMSO for dimethyl sulfoxide, DIPEA for N,N-diisopropylethylamine, FCC for flash column chromatography, MeOH for methanol, TEA for triethylamine, DMF for N,N-dimethylformamide, HATU for 1-[bis(dimethylamino)methylene]-1H-1,2,3-triazolo[4,5-b]pyridinium 3-oxid hexafluorophosphate, TFA for trifluoroacetic acid.

(S)-4-((2-(2-(benzyloxy)ethoxy)ethoxy)methyl)-2,2-dimethyl-1,3-dioxolane (5)

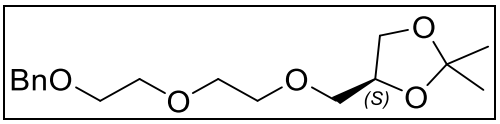

To a solution of (*S*)-(+)-1,2-isopropylideneglycerol **3** (1.6 g, 12.0 mmol) in dioxane (40 mL) freshly ground KOH (740 mg, 13.2 mmol) was added, followed by 2-(2-(benzyloxy)ethoxy)ethyl 4-methylbenzenesulfonate **4** (7.0 g, 20 mmol) and a catalytic amount of tetrabutylammonium iodide. The mixture was stirred at 105 °C overnight. The solvent was removed under reduced pressure, a saturated solution of ammonium chloride (50 mL) was added to the residue and the mixture was extracted with DCM (3 x 100 mL). The collected organic phase was dried on anhydrous $MgSO_4$, evaporated to dryness and the crude was purified by FCC using a gradient from 10% to 50% of EtOAc in heptane. Obtained 1.94 g, 52% (transparent oil).

^{1}H-NMR (500 MHz, $CDCl_3$) δ: 7.35 - 7.25 (m, 5H), 4.27 (td, *J*=6.0, 12.0 Hz, 1H), 4.04 (dd, *J*=6.4, 8.2 Hz, 1H), 3.74 - 3.61 (m, 9H), 3.58 (dd, *J*=5.9, 9.8 Hz, 1H), 3.50 (dd, *J*=5.7, 10.0 Hz, 1H), 1.41 (s, 3H), 1.35 (s, 3H).

^{13}C-NMR (12.5.77 MHz, $CDCl_3$) δ: 138.2, 128.3, 127.7, 127.6, 109.3, 74.7, 73.2, 72.4, 71.0, 70.7, 70.6, 69.4, 66.8, 26.8, 25.4.

(R)-3-(2-(2-(benzyloxy)ethoxy)ethoxy)propane-1,2-diol (6)

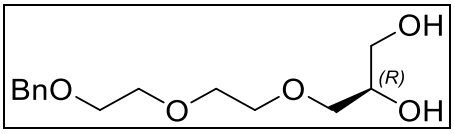

The acetonide **5** (1.94 g, 6.25 mmol) was dissolved in 80% aqueous acetic acid (40 mL) and stirred until complete consumption of the starting material was observed by TLC (50% of EtOAc in heptane). The reaction mixture was evaporated to dryness to obtain the desired product in quantitative yield (1.68 g) as a transparent oil.

^{1}H-NMR (500 MHz, $CDCl_3$) δ: 7.35 - 7.27 (m, 5H), 4.57 (s, 2H), 3.88 - 3.83 (m, 1H), 3.70 - 3.54 (m, 12H), 2.08 - 2.07 (m, 1H).

^{13}C-NMR (125.77 MHz, $CDCl_3$) δ: 138.0, 128.4, 127.8, 127.7, 73.3, 73.0, 70.8, 70.6, 70.5, 69.4, 63.9.

(S)-13,13,14,14-tetramethyl-1-phenyl-2,5,8,12-tetraoxa-13-silapentadecan-10-ol (7)

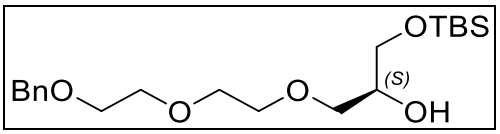

A solution of **6** (1.68 g, 6.25 mmol) in anhydrous DCM (7 mL) was cooled at 0 °C. TEA (1.2 mL, 8.75 mmol) and DMAP (46 mg, 0.375 mmol) were added, followed by a dropwise addition of TBSCl (1.32 g, 8.75 mmol) in DCM (8 mL). The reaction was allowed to reach r.t. overnight while stirring, then the reaction mixture was quenched with water (20 mL) and extracted with DCM. The organic layer was dried over $MgSO_4$ and evaporated to dryness. The crude product was purified by FCC using a gradient from 20% to 50% of EtOAc in heptane. Obtained 2.0 g, 83% yield (transparent oil).

^{1}H-NMR (500 MHz, $CDCl_3$) δ: 7.35 - 7.27 (m, 5H), 4.57 (s, 2H), 3.85 - 3.79 (m, 1H), 3.69 - 3.62 (m, 10H), 3.57 (dd, *J*=4.7, 10.0 Hz, 1H), 3.50 (q, *J*=5.3 Hz, 1H), 2.65 (d, *J*=4.8 Hz, 1H), 0.89 (s, 9H), 0.06 (s, 6H).

^{13}C-NMR (125.77 MHz, $CDCl_3$) δ: 138.2, 128.4, 127.8, 127.6, 73.3, 72.3, 70.9, 70.7, 70.6, 69.4, 64.0, 25.9, 18.3, -5.4.

(R)-10-azido-13,13,14,14-tetramethyl-1-phenyl-2,5,8,12-tetraoxa-13-silapentadecane (8)

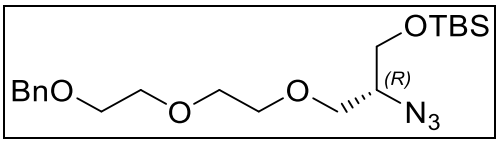

To a solution of **7** (2.0 g, 5.2 mmol) in anhydrous pyridine (11 mL), mesyl chloride (0.800 mL, 10.4 mmol) was added dropwise. The was allowed to reach r.t. overnight while stirring, then the reaction mixture was quenched with saturated sodium bicarbonate (20 mL) and extracted with DCM. The organic layer was dried over $MgSO_4$ and concentrated before being dissolved in DMF (20 mL). Sodium azide (1.39 g, 26 mmol) was added and the reaction mixture was heated at 100

°C overnight. The reaction mixture was then allowed to cool to r.t., saturated sodium bicarbonate (20 mL) was added the mixture was extracted with EtOAc. The organic layer was dried over $MgSO_4$ and concentrated. The crude was then purified by FCC using a gradient from 0% to 50% of EtOAc in heptane. Obtained 0.95 g, 45% yield over two steps (transparent oil).

^{1}H-NMR (400 MHz, $CDCl_3$) δ: 7.35 - 7.26 (m, 5H), 4.57 (s, 2H), 3.77 - 3.52 (m, 13H), 0.90 (s, 9H), 0.08 (s, 6H).

^{13}C-NMR (100.62 MHz, $CDCl_3$) δ: 138.2, 128.3, 127.7, 127.6, 73.2, 70.9, 70.7, 70.6, 70.5, 69.4, 63.3, 62.3, 25.8, 18.2, -5.6.

(R)-10-azido-1,1,1,19-tetraphenyl-2,5,8,12,15,18-hexaoxanonadecane (10)

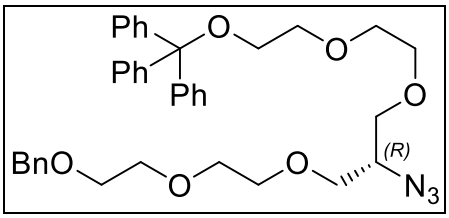

To a solution of **8** (952 mg, 2.06 mmol) in anhydrous THF (10 mL) a solution of TBAF (1 M in THF, 6.2 mL) was added dropwise at 0 °C. The ice bath was removed and the reaction mixture was allowed to stir at r.t. until complete consumption of the starting material was observed by TLC (40% of EtOAc in heptane). A saturated solution of ammonium chloride (10 mL) was added the mixture was extracted with DCM. The organic layer was dried over $MgSO_4$ and concentrated. ^{1}H-NMR (500 MHz, $CDCl_3$) d: 7.35 - 7.27 (m, 5H), 4.57 (s, 2H), 3.78 - 3.62 (m, 14H), 2.29 (t, *J*=6.2 Hz, 1H)].

The deprotected alcohol (620 mg, 2.0 mmol) was then dissolved in dioxane (20 mL), freshly ground KOH (168 mg, 3 mmol) was added, followed by 2-(2-(trityloxy)ethoxy)ethyl methanesulfonate [5] (**9**, 980 mg, 2.3 mmol) and TBAI (85 mg, 0.23 mmol). The mixture was stirred at 105 °C overnight. ~The mixture was allowed to cool to r.t., then brine (20 mL) was added and the mixture was extracted with DCM (3 x 100 mL). The collected organic phase was dried on anhydrous $MgSO_4$, evaporated to dryness and the crude was purified by FCC using a gradient from 10% to 70% of EtOAc in heptane. Obtained 1.32 g, 97% yield (transparent oil).

^{1}H-NMR (400 MHz, $CDCl_3$) δ: 7.41 - 7.36 (m, 7H), 7.27 - 7.12 (m, 16H), 4.49 (s, 1H), 3.67 - 3.44 (m, 20H), 3.17 (t, *J*=4.8 Hz, 2H).
^{13}C-NMR (100.62 MHz, $CDCl_3$) δ: 144.2, 138.3, 128.7, 128.4, 127.8, 127.7, 127.6, 126.9, 86.6, 73.3, 71.1, 71.0, 70.8, 70.6, 69.5, 63.4, 60.7.

(S)-10-azido-1-phenyl-2,5,8,12,15-pentaoxaheptadecan-17-ol (11)

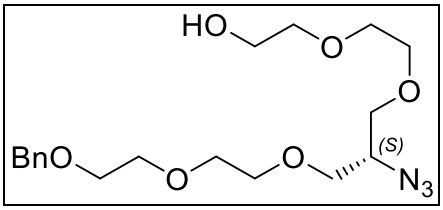

To a solution of **10** (600 mg, 0.95 mmol) in DCM (9 ml) TFA (1 mL) was added, followed by TIPS (1mL). The reaction mixture was stirred for 20 minutes, TLC (40% of EtOAc in heptane) analysis showed complete consumption of the starting material. The reaction was quenched with a saturated solution of $NaHCO_3$ and extracted with DCM. The collected organic phase was dried on anhydrous $MgSO_4$, evaporated to dryness and the crude was purified by FCC using a gradient from 20% to 100% of EtOAc in heptane. Elution of the desired product was obtained with 100% EtOAc. Obtained 280 mg, 77% yield (transparent oil).
^{1}H-NMR (500 MHz, $CDCl_3$) δ: 7.35 - 7.28 (m, 5H), 4.58 (s, 2H), 3.80 - 3.55 (m, 22H).
^{13}C-NMR (100.62 MHz, $CDCl_3$) δ: 138.3, 128.4, 127.7, 127.6, 73.3, 72.4, 71.0, 70.9, 70.8, 70.7, 70.6, 70.4, 69.5, 61.8, 60.6.

tert-butyl (R)-10-azido-1-phenyl-2,5,8,12,15,18-hexaoxaicosan-20-oate (12)

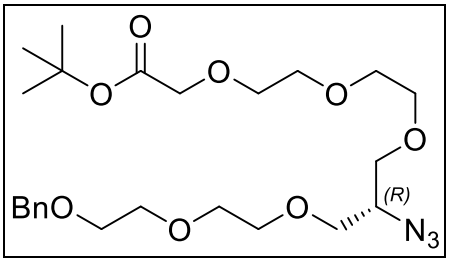

To a stirred solution of **11** (271 mg, 0.70 mmol) in DCM (1.5 mL) a solution of 37% NaOH (1.5 ml) was added, followed by *tert*-butylbromo acetate (546 mg, 2.8 mmol) and TBABr (230 mg, 0.71 mmol). The resulting solution was stirred overnight at r.t. The reaction mixture was diluted with water and extracted with DCM. The organic phase was over $MgSO_4$ and concentrate in vacuo. The resulting oil was purified by FCC using a gradient from 20% to 100% of EtOAc in heptane. Yield: 246 mg, 71%, transparent oil.

^{1}H-NMR (500 MHz, $CDCl_3$) δ: 7.35 - 7.27 (m, 5H), 4.57 (s, 2H), 4.01 (s, 2H), 3.74 - 3.53 (m, 21H), 1.48 (s, 9H).

^{13}C-NMR (125.77 MHz, $CDCl_3$) δ: 169.6, 138.3, 128.3, 127.7, 127.6, 81.5, 73.2, 71.0, 70.9, 70.7, 70.6, 70.5, 69.5, 69.0, 60.6, 28.1.

tert-butyl (R)-11-((2-(2-hydroxyethoxy)ethoxy)methyl)-13-oxo-3,6,9,14-tetraoxa-12-azaheptadec-16-enoate (13)

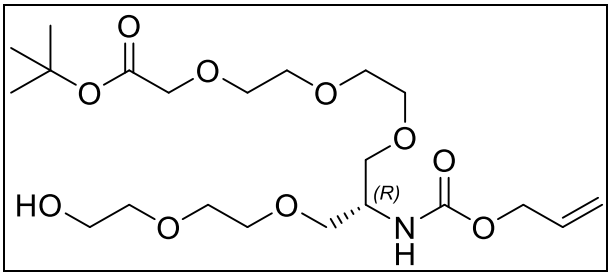

A solution of **12** (240 mg, 0.48 mmol) in ethanol (0.05 M) containing 5% of acetic acid was hydrogenated at 90 bar in a H-Cube (ThalesNano, 10% Pd/C cartridge) using a flow of 0.25 mL/min, 70 °C. The solvent was removed under reduced pressure and the crude was dissolved in dioxane/water (2:1, 3 mL). $NaHCO_3$ (130 mg, 1.53mmol) and *N*-(allyloxycarbonyloxy)succinimide (123 mg, 0.614 mmol) were added and the reaction was stirred at room temperature overnight .The reaction mixture was extracted with DCM, the organic phase was over $MgSO_4$ and concentrate in vacuo. The crude was purified by by FCC using a gradient from 0% to 10% of MeOH in DCM. Yield: 197 mg, 88% over two steps, transparent glass.

^{1}H-NMR (500 MHz, $CDCl_3$) δ: 5.96 - 5.86 (m, 1H), 5.47 (d, *J*=7.5 Hz, 1H), 5.32 - 5.19 (m, 3H), 4.58 - 4.52 (m, 2H), 4.01 (s, 2H), 3.74 - 3.49 (m, 21H), 1.45 (s, 9H).

^{13}C-NMR (100.62 MHz, $CDCl_3$) δ: 169.6, 155.9, 132.9, 117.7, 81.5, 72.5, 70.7, 70.6, 70.5, 70.4, 69.7, 69.6, 69.0, 65.7, 65.5, 61.8, 50.2, 28.1. MS analysis: m/z = 466.3 $[M+H]^+$, expected for $C_{21}H_{39}NO_{10}$: 465.3.

tert-butyl (S)-11-((2-(2-(2-(((2S,4R)-1-((S)-2-((tert-butoxycarbonyl)amino)-3,3-dimethylbutanoyl)-4-hydroxypyrrolidine-2-carboxamido)methyl)-5-(4-methylthiazol-5-yl)phenoxy)ethoxy)ethoxy)methyl)-13-oxo-3,6,9,14-tetraoxa-12-azaheptadec-16-enoate (16)

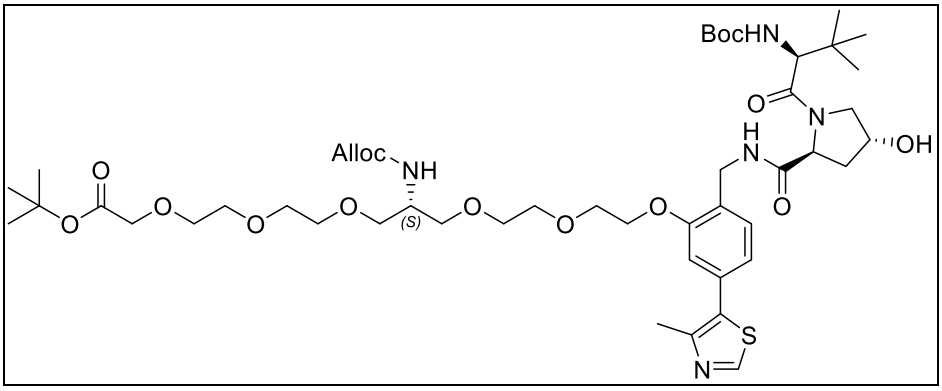

To a solution of **13** (187 mg, 0.40 mmol) in DCM (3 mL) at 0 °C, TEA (84 µL, 0.60 mmol) was added, followed by mesyl chloride (37 µL, 0.48 mmol). The reaction mixture was stirred at 0 °C for 10 minutes and then allowed to reach r.t. over 3 h. A 5% solution of $NaHCO_3$ was added, the reaction mixture was extracted with DCM, the organic phase was over $MgSO_4$ and concentrate in vacuo to give the mesylate linker which was immediately dissolved in anhydrous DMF (2 mL). Compound **15** [6] (145 mg, 0.27 mmol) was added to the mesylate solution, followed by freshly ground anhydrous K_2CO_3 (110 mg, 0.80 mmol). The reaction mixture was vigorously stirred at 75 °C overnight. The reaction mixture was then allowed to cool to r.t., diluted with DCM and filtered over a celite pad. Volatiles were removed under reduced pressure and the crude was purified by FCC using a gradient from 0% to 15% of MeOH in DCM. Yield: 169 mg, 64% over two steps, transparent glass.

^{1}H-NMR (400 MHz, MeOD) δ: 8.89 (s, 1H), 7.48 (d, *J*=7.8 Hz, 1H), 6.37 (d, *J*=9.5 Hz, 1H), 5.97 - 5.87 (m, 1H), 5.34 - 5.15 (m, 3H), 4.63 (t, *J*=8.3 Hz, 1H), 4.57 - 4.37 (m, 7H), 4.32 - 4.23 (m, 4H), 4.02 (s, 2H), 3.94 - 3.86 (m, 5H), 3.82 - 3.74 (m, 4H), 3.69 - 3.53 (m, 21H), 2.50 (s, 3H), 2.26 - 2.20 (m, 1H), 2.15-2.05 (m, 1H), 1.48 (s, 9), 1.45 (s, 9H), 1.00 (s, 9H).

^{13}C-NMR (100.62 MHz, MeOD) δ: 173.1, 171.9, 158.3, 153.2, 149.4, 134.8, 133.8, 133.1, 130.3, 128.7, 123.2, 117.9, 114.1, 83.0, 81.0, 72.0, 72.0, 71.8, 71.8, 71.5, 71.4, 71.2, 70.1, 69.7, 66.7, 61.0, 60.6, 58.3, 52.4, 39.8, 39.1, 37.1, 29.0, 28.7, 27.2, 16.2. MS analysis: m/z = 994.5 $[M+H]^+$, expected for $C_{48}H_{75}N_5O_{15}S$: 993.5.

allyl ((2R,6S,18S,33aS)-6-(tert-butyl)-2-hydroxy-28-(4-methylthiazol-5-yl)-5,8,33-trioxo-2,3,6,7,8,9,11,12,14,15,18,19,21,22,24,25,31,32,33,33a-icosahydro-1H,5H,17H-benzo[r]pyrrolo[1,2-m][1,4,7,20,23,26]hexaoxa[10,13,16]triazacyclononacosin-18-yl)carbamate (17)

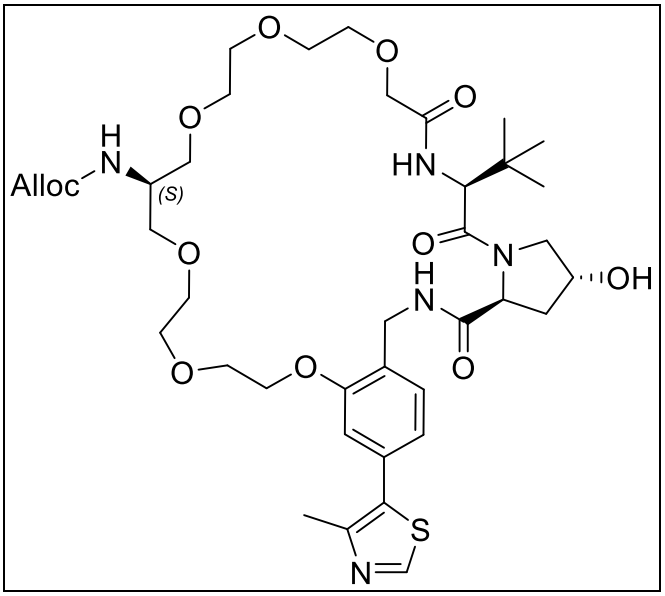

Compound **16** (169 mg, 0.17 mmol) was dissolved in a mixture of TFA/DCM (1:1, 3 mL). The reaction was stirred for 3 h, then volatile components were evaporated under reduced pressure. The reside was taken up with 0.1 M aqueous HCl (15 mL), frozen and freeze dried to obtain the HCl salt which was then dissolved in a mixture of anhydrous DCM (50 mL) and DIPEA (110 µL, 0.63 mmol). This solution was added dropwise to a solution of HATU (162 mg, 0.425 mmol) and DIPEA (55 µL, 0.32 mmol) in DCM (50 mL). The reaction mixture was stirred overnight. Solvent was removed and the crude was purified by FCC using a gradient from 0% to 20% of MeOH in DCM. Yield: 105 mg, 75% over two steps, transparent glass.

^{1}H-NMR (400 MHz, MeOD) δ: 8.89 (s, 1H), 8.22 (t, *J*=5.7 Hz, 1H), 7.67 (d, *J*=10.3 Hz, 1H), 7.36 (d, *J*=8.0 Hz, 1H), 7.08 (d, *J*=1.3 Hz, 1H), 7.03 (d, *J*=1.7 Hz, 1H), 7.02 (d, *J*=1.4 Hz, 1H), 5.97 -

5.87 (m, 1H), 5.29 (dd, *J*=1.5, 17.2 Hz, 1H), 5.15 (d, *J*=10.6 Hz, 1H), 4.74 (d, *J*=9.7 Hz, 1H), 4.63 - 4.44 (m, 5H), 4.39 - 4.28 (m, 2H), 4.19 - 4.12 (m, 1H), 4.02 (s, 2H), 3.98 - 3.53 (m, 23H), 2.52 (s, 3H), 2.23 - 2.16 (m, 1H), 1.97 - 1.90 (m, 1H), 1.05 (s, 9H).
^{13}C-NMR (100.62 MHz, MeOD) δ: 174.3, 172.2, 172.1, 171.4, 158.8, 153.2, 149.5, 134.7, 133.6, 131.4, 129.3, 123.3, 117.9, 115.0, 72.7, 72.3, 71.9, 71.8, 71.6, 71.4, 71.2, 70.7, 69.8, 60.8, 58.3, 52.6, 40.4, 39.1, 37.8, 27.3, 16.2. MS analysis: m/z = 820.4 $[M+H]^+$, expected for $C_{39}H_{57}N_5O_{12}S$: 819.4.

(2R,6S,18S,33aS)-18-amino-6-(tert-butyl)-2-hydroxy-28-(4-methylthiazol-5-yl)-1,2,3,6,7,11,12,14,15,18,19,21,22,24,25,31,32,33a-octadecahydro-5H,17H,33H-benzo[r]pyrrolo[1,2-m][1,4,7,20,23,26]hexaoxa[10,13,16]triazacyclononacosine-5,8,33(9H)-trione (18)

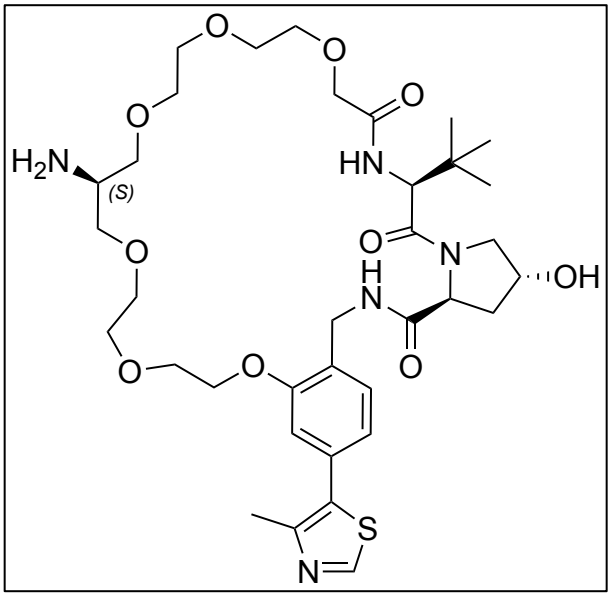

To a solution of **17** (35mg, 0.043 mmol) in THF (3 mL), $Pd(PPh_3)_4$ (5 mg, 0.0043 mmol) and phenylsilane (53 μL, 0.43 mmol) were added. The reaction was stirred for 20 minutes at r.t., dried over reduced pressure and the reside was dissolved in methanol, filtered and purified by preparative HPLC using a gradient from 5% to 95% of acetonitrile in water containing 0.01% of ammonium hydroxide over 15 minutes. The fractions congaing the product were freeze dried to obtain the desired product, 19 mg (63 %) as a white solid.

^{1}H-NMR (400 MHz, DMSO-D6) δ: 8.97 (s, 1H), 8.45 - 8.40 (m, 1H), 7.38 (d, *J*=9.4 Hz, 1H), 7.20 (d, *J*=7.6 Hz, 1H), 7.05 (d, *J*=1.5 Hz, 1H), 7.01 (dd, *J*=1.4, 7.8 Hz, 1H), 4.60 - 4.43 (m, 3H), 4.35 (s, 1H), 4.26 - 4.07 (m, 4H), 3.93 (s, 2H), 3.78 (t, *J*=5.3 Hz, 2H), 3.64 - 3.25 (m, 24H), 3.07 - 3.00 (m, 1H), 2.47 (s, 3H), 2.14 - 2.07 (m, 1H), 1.96 - 1.87 (m, 1H), 0.96 (s, 9H).
^{13}C-NMR (100.62 MHz, DMSO-D6) δ: 172.1, 169.4, 168.9, 165.0, 156.4, 151.9, 148.4, 131.7, 131.4, 128.0, 121.7, 113.1, 72.9, 72.7, 71.5, 70.6, 70.5, 70.4, 70.1, 70.0, 69.4, 69.3, 68.6, 59.3, 57.2, 56.2, 50.7, 38.3, 37.4, 36.5, 26.7, 16.5. MS analysis: m/z = 736.4 $[M+H]^+$, expected for $C_{35}H_{53}N_5O_{10}S$: 735.4.

N-((2R,6S,18S,33aS)-6-(tert-butyl)-2-hydroxy-28-(4-methylthiazol-5-yl)-5,8,33-trioxo-2,3,6,7,8,9,11,12,14,15,18,19,21,22,24,25,31,32,33,33a-icosahydro-1H,5H,17H-benzo[r]pyrrolo[1,2-m][1,4,7,20,23,26]hexaoxa[10,13,16]triazacyclononacosin-18-yl)-2-((S)-4-(4-chlorophenyl)-2,3,9-trimethyl-6H-thieno[3,2-f][1,2,4]triazolo[4,3-a][1,4]diazepin-6-yl)acetamide (1)

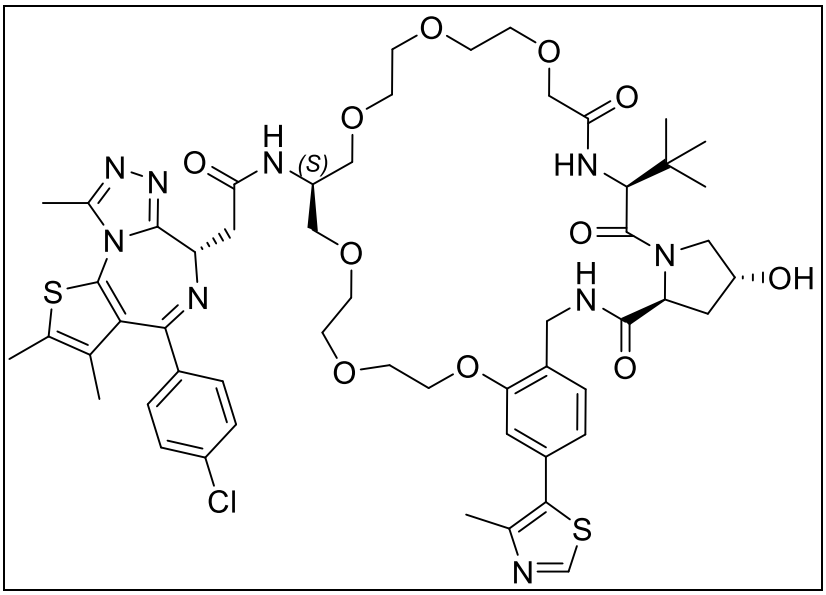

To a solution of amine **17** (10 mg, 0.136 mmol), (+)-JQ1-COOH [7] (5.5 mg, 0.0136 mmol) in DMF (1 mL), DIPEA (5 μL, 0.0272 mmol) and COMU (6 mg, 0.0136 mmol) were added. The reaction was stirred at r.t. for 1 h. Methanol (0.5 mL) was added and the crude mixture was purified

by preparative HPLC using a gradient from 5% to 95% of acetonitrile in water containing 0.01% of ammonium hydroxide over 15 minutes. The fractions congaing the product were freeze dried to obtain the desired product, 8 mg (52%) as a white solid.

^{1}H-NMR (400 MHz, MeOD) δ: 8.87 (s, 1H), 7.47 (d, *J*=8.5 Hz, 2H), 7.41 (d, *J*=8.5 Hz, 2H), 7.33 (d, *J*=7.9 Hz, 1H), 7.06 (d, *J*=1.4 Hz, 1H), 6.97 (dd, *J*=1.5, 7.8 Hz, 1H), 4.71 (s, 1H), 4.63 - 4.56 (m, 3H), 4.45 - 4.42 (m, 1H), 4.39 - 4.31 (m, 2H), 4.28 (t, J=5.6 Hz, 1H), 4.21 - 4.16 (m, 1H), 4.03 (s, 2H), 3.99 - 3.87 (m, 2H), 3.81 - 3.58 (m, 18H), 3.47 - 3.41 (m, 1H), 2.67 (s, 3H), 2.48 (s, 3H), 2.45 (s, 3H), 2.20 - 2.14 (m, 1H), 2.01 - 1.94 (m, 1H), 1.71 (s, 3H), 1.04 (s, 9H).

^{13}C-NMR (100.62 MHz, MeOD) δ: 174.4, 173.0, 172.1, 171.4, 166.3, 158.7, 157.3, 153.2, 152.4, 149.5, 138.4, 138.2, 133.4, 132.4, 131.7, 131.0, 130.1, 129.0, 123.1, 114.6, 72.7, 72.2, 72.1, 71.9, 71.4, 71.3, 71.2, 70.9, 69.8, 60.9, 58.3, 55.5, 50.9, 40.2, 39.1, 37.8, 27.4, 16.3, 14.7, 13.2, 11.9.

HRMS analysis: m/z = N1118.4334 $[M+H]^{+}$, 559.7168 $[M+2H]^{2+}$ expected for $C_{54}H_{68}ClN_9O_{11}S_2$: 1117.4168.

Protein expression and purification

Wild-type versions of human proteins VHL (UniProt accession number: P40337), ElonginC (Q15369), ElonginB (Q15370), Brd2 (P25440), Brd3 (Q15059) and Brd4 (O60885) were used for all protein expression. For expression of VCB, N-terminally His_6-tagged VHL (54–213), ElonginC (17–112) and ElonginB (1–104) were co-transformed into *Escherichia coli* BL21(DE3) and grown at 37 °C. Upon reaching an OD_{600} ~ 1.0, the temperature was lowered to 23 °C and expression was induced using 0.3 mM isopropyl β-D-1-thiogalactopyranoside (IPTG). Sixteen hours post-induction, *E. coli* cells were lysed using a pressure cell homogenizer (Stansted Fluid Power) and the lysate was clarified by centrifugation. His_6-tagged VCB was purified on a HisTrap FF affinity column (GE Healthcare) by elution with an imidazole gradient. The His_6-tag was then removed using TEV protease (overnight, 4 °C) and protein was reapplied to the HisTrap FF column, allowing impurities to bind and the cleaved complex to flowthrough without binding. VCB was then additionally purified by anion exchange and size-exclusion chromatography using Resource Q and Superdex-75 columns (GE Healthcare), respectively. The final purified complex was stored in 20 mM 4-(2-hydroxyethyl)-1-piperazineethanesulfonic acid (HEPES) (pH 7.5) 100 mM sodium chloride and 1 mM TCEP.

$Brd2^{BD1}$ (71–194), $Brd2^{BD2}$ (344-455), $Brd3^{BD1}$ (24-146), $Brd3^{BD2}$ (306-416), $Brd4^{BD1}$ (44-178) and $Brd4^{BD2}$ (333–460) were expressed with an N-terminal His_6 tag in *E. coli* BL21(DE3) at 15 °C for 18 h using 0.3 mM IPTG. Cells were lysed as above, and His_6-tagged BDs were purified on Nickel Sepharose 6 fast flow beads (GE Healthcare) by elution with imidazole. Eluted BDs were then additionally purified by size-exclusion chromatography using a Superdex-75 column. The final purified proteins were stored in 20 mM HEPES (pH 7.5), 100 mM sodium chloride and 1 mM TCEP. All chromatography purification steps were performed using Äkta FPLC purification systems (GE Healthcare) or glass econo-columns (Bio-Rad) at room temperature.

Isothermal titration calorimetry (ITC)

The titrations were all performed as reverse mode (protein in syringe, ligand in cell) and consisted of 19 injections of 2 µl protein solution (20 mM bis–tris propane, 100 mM NaCl, 1 mM tris(2-carboxyethyl)phosphine (TCEP), pH 7.4) at a rate of 0.5 µl/s at 120 s time intervals. An initial

injection (0.4 µl) was made and discarded during data analysis. All experiments were performed at 25 °C, whilst stirring at 600 r.p.m.

PROTAC **1** was diluted from a 10 mM DMSO stock solution to 20 µM in buffer containing 20 mM bis-tris propane, 100 mM NaCl, 1 mM tris(2-carboxyethyl)phosphine (TCEP), pH 7.4. The final DMSO concentration was 0.2 %. Bromodomain (200 µM, in the syringe) was titrated into **1** (20 µM, in the cell). At the end of the titration, the excess of solution was removed from the cell, the syringe was washed and dried, VCB complex (168 µM, in the same buffer) was loaded in the syringe and titrated into the complex PROTAC–bromodomain.

Titrations for the binary complex **1**–VCB were performed as follows: to the solution of **1** (20 µM, in the cell), buffer (38.4 µL) was added by means of a single ITC injection. The excess solution was removed from the cell, the syringe was washed and dried and VCB complex (168 µM, in the same buffer) was loaded in the syringe and titrated into the diluted PROTAC solution. The data were fitted to a single-binding-site model to obtain the stoichiometry n, the dissociation constant K_d and the enthalpy of binding ΔH using the d analyzed using the MicroCal PEAQ-ITC analysis software provided by the manufacturer. Cooperativity (α) values were calculated from the ratio of binary K_d and ternary K_d values determined for VCB binding to **1** or **1**:bromodomain, respectively. The reported values are the mean ± standard deviation from independent measurements.

Fluorescence polarization assay

FP competitive binding assays were run in triplicate on 384-well plates [Corning 3575] as described previously,[8] with all measurements taken using a PHERAstar FS (BMG LABTECH) with fluorescence excitation and emission wavelengths (λ) of 485 and 520 nm, respectively. The final assay volume was 15 μL, with each well solution containing 15 nM VCB protein, 10 nM FAM-labeled HIF-1α peptide (FAM-DEALAHypYIPMDDDFQLRSF, "JC9") and decreasing concentrations of PROTAC (14-point 2-fold serial dilution starting from 50 μM) or PROTAC:bromodomain (14-point 2-fold serial dilutions starting from 10 μM PROTAC:20 μM bromodomain). All components were dissolved from stock solutions using 100 mM Bis-Tris propane, 100 mM NaCl, 1 mM TCEP, pH 7.5, and DMSO was added as appropriate to ensure a final concentration of 1%. Control wells containing VCB and JC9 with no compound (zero displacement), or JC9 in the absence of protein (maximum displacement) were also included. Data were normalized to control values in order to obtain percentage displacements, which were then plotted against Log[PROTAC]. Curves were fitted by nonlinear regression using Prism (v. 8.0.1, GraphPad) to determine the IC_{50} values for each titration. K_i values were back-calculated from the K_d for JC9 (~2 nM, determined from direct binding) and fitted IC_{50} values, as described previously. Cooperativity (α) values were calculated from the ratio of binary K_i and ternary K_i values determined for JC9 displacement by 1 alone or 1 + bromodomain, respectively.

Crystallography

The ternary complex VCB:**1**:$Brd4^{BD2}$ was prepared by combining VCB, $Brd4^{BD2}$, and **1** in a 1:1:1 molar ratio and incubating for 15 min at RT. Crystals were grown at 20 °C using the hanging-drop diffusion method by mixing equal volumes of ternary complex solution and a crystallization solution containing 10% (w/v) PEG 8000, 0.1 M Tris-HCl (pH 7.5) and 0.1 M $MgCl_2$. Crystals appeared almost immediately, and were ready for harvest within 24 h. Crystals were flash-frozen in liquid nitrogen using 20% (v/v) ethylene glycol in liquor solution as a cryoprotectant. Diffraction data were collected at Diamond Light Source beamline I04 using a Pilatus 6M-F detector at a wavelength of 0.9750 Å. Reflections were indexed and integrated using XDS [9], and scaling and merging were performed with AIMLESS [10] in CCP4i.[11] The crystals belonged to space group $P3_2$, and there were two copies of the ternary complex in the asymmetric unit. The

structure was solved by molecular replacement using PHASER MR [12] and search models derived from the coordinates for the VCB:MZ1:Brd4^{BD2} ternary complex (PDB entry 5T35). The initial model underwent iterative rounds of model building and refinement with COOT [13] and REFMAC5,[14] respectively. All riding hydrogens were excluded from the output coordinate files but included for refinement. Compound **1** geometry restraints for refinement were prepared with the PRODRG [15] server and optimized using eLBOW [16] from the PHENIX suite.[17] Model geometry and steric clashes were validated using the MOLPROBITY server.[18] Ramachandran plots indicate that 96.8% of backbone torsion angles are in the favored region and there are no outliers. The structure has been deposited in the protein data bank (PDB) with accession code 6SIS; data collection and refinement statistics are presented in table S2. Interfaces observed in the crystal structure were calculated using PISA, and all figures were generated using PyMOL.

	VCB:**1**:Brd4^{BD2}
Data Collection	
Space Group	$P3_2$
Cell Dimensions	
a, b, c (Å)	99.5 99.5 148.4
α, β, γ, (°)	90 90 120
Resolution (*Å)*	49.7 – 3.50 (3.83 – 3.50)*
No. unique reflections	19215 (4396)
R_{merge} (%)	13.5 (58.7)
$I/\sigma(I)$	6.3 (1.5)
$CC_{1/2}$	0.984 (0.542)
Completeness (%)	92.6 (88.4)
Redundancy	2.6 (2.6)
Refinement	
Resolution	49.7 – 3.5
R_{work} / R_{free}	22.0 / 24.7
No. atoms	
Protein	7208
Ligand	154
Water	7
B factors	
Protein	112
Ligand	90
Water	37
R.m.s. deviations	
Bond lengths (Å)	0.005
Bond angles (°)	0.729
Buried surface area (Å).	
VHL:Brd4^{BD2}	661
VHL:**1**	961
Brd4^{BD2}:**1**	1064

Table S2 *Crystallographic data collection and refinement statistics. * Values in parentheses are for highest-resolution shell.*

Tissue culture

HeLa cells were kept in DMEM (Gibco) supplemented with 10%(v/v) FBS (Gibco), 2 mM L-glutamine (Gibco), penicillin (100 units /mL) and streptomycin (100 µg/mL) (Gibco). Mv4;11 and 22RV1 (ATCC CRL-2505) cells were kept in RPMI 1640 supplemented with 10% (v/v) FBS (Gibco), 2 mM L-glutamine (Gibco), penicillin (100 units /mL) and streptomycin (100 µg/mL) (Gibco). Cells were kept at 37 °C, 5% CO_2.

Testing compounds in cells

HeLa cells or 22RV1 cells (6 x 10^5) were seeded onto each well on a six-well plate 24 h before treatment with test compounds. To treat the cells with the test compounds, medium was replaced with fresh medium containing specified concentration of test compounds for either 4 h or 18 h. The same DMSO concentration was maintained in all samples. At the end of treatment, cells were washed with PBS and then lysed in RIPA buffer (Sigma, R0278) supplemented with HALT Protease inhibitor (ThermoFisher, # 78842). Lysate was incubated on ice for 15 minutes on ice and then clarified by centrifugation (20,000 x *g*, 10 min, 4 °C). Supernatant was collected and protein concentration was determined by BCA assay. The rest of the clarified lysate was kept at -80°C before further processing.

Immunoblotting

Protein on gel was transferred to nitrocellulose membrane using the Bio-Rad Transblot system according to manufacturer guidelines. Blots were probed with anti-Brd4 (AbCam, ab128874), anti-Brd3 (AbCam, ab50818), anti-Brd2 (AbCam, ab139690) and anti-c-MYC (Y69 ab32072) followed by hFAB™ Rhodamine Anti-Tubulin (Biorad #12004165) and anti-mouse IgG (Licor, 926-32210) or anti-rabbit IgG (Licor, 926-32213) antibodies and bands visualized using Bio-Rad ChemiDoc MP Imaging System.

Western Blot Quantification

Image processing and band intensity quantification were performed using Bio-Rad Image Lab

software version 6.0.0. Reported band intensities are first normalized to tubulin loading control and then to DMSO only treated sample.

Cell Viability Assay

MV4;11 or 22RV1 cells (15000 or 5000 cells per well respectively) were dosed for 48 or 72 h with compounds serially diluted (1:3) on a clear-bottom 384-well plate with a final concentration of 0.05% (v/v) DMSO. After treatment, Promega CellTiter-Glo luminescent cell viability assay (G7572) was added to the cells according to the manufacturer instructions. The signal from each well was recorded on a BMG Labtech Pherastar luminescence plate reader with recommended settings. Normalized data were analyzed and plotted with Graphpad Prism software in the 'log(inhibitor) vs. response -- Variable slope (four parameters)' module. EC50 values of each test compound were derived from this plot.

	MZ1	**1**	cis-MZ1
MV4;11 EC50 (nM) 48 h	149	304	N/A
MV4;11 EC50 (nM) 72 h	7	47	1420
22RV1 EC50 (nM) 72 h	191	643	1457

Copies of NMR spectra

Compound **5**, ^{1}H-NMR $CDCl_3$, 500 MHz

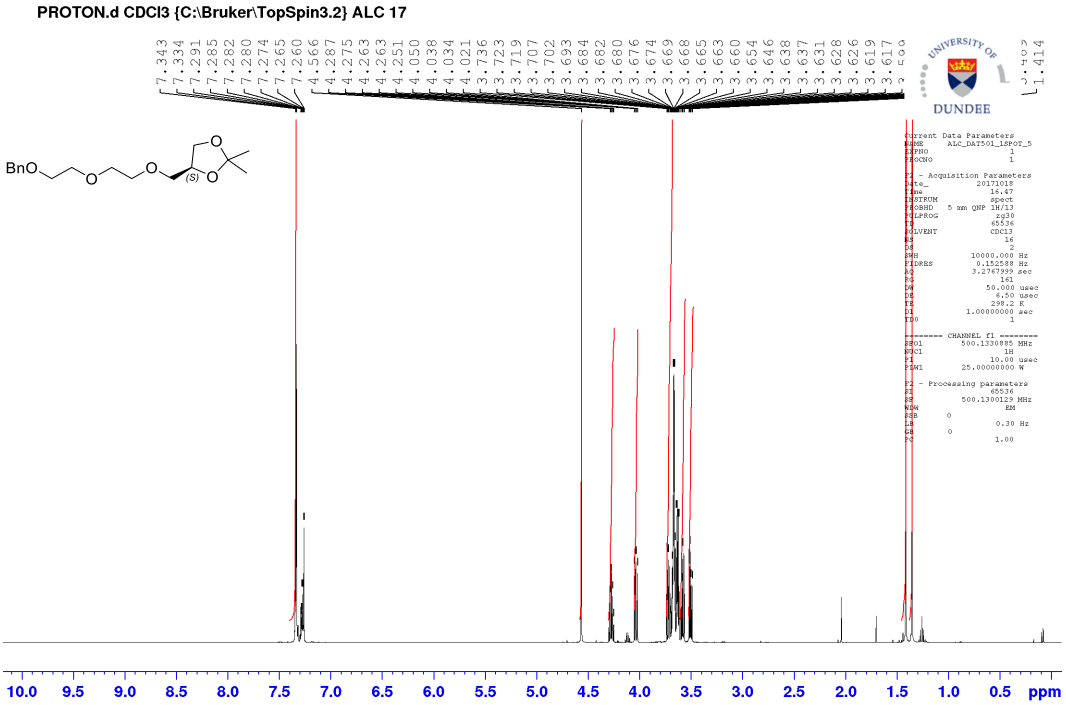

Compound **5**, ^{13}C-NMR $CDCl_3$, 126 MHz

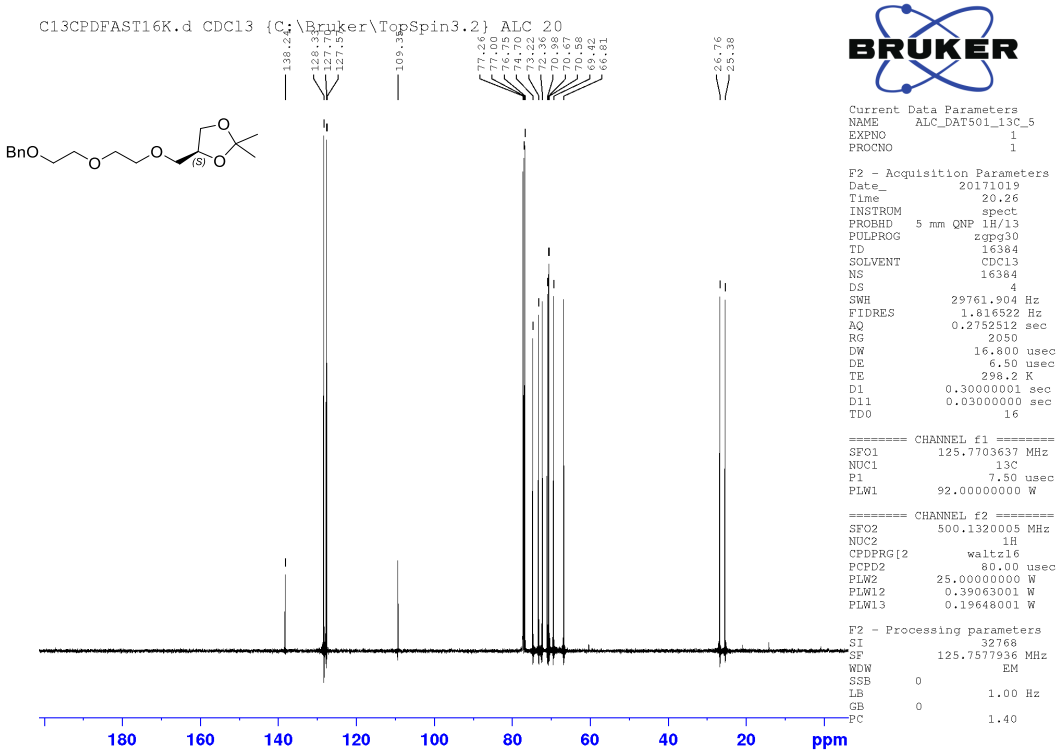

Compound **6**, ^{1}H-NMR $CDCl_3$, 500 MHz

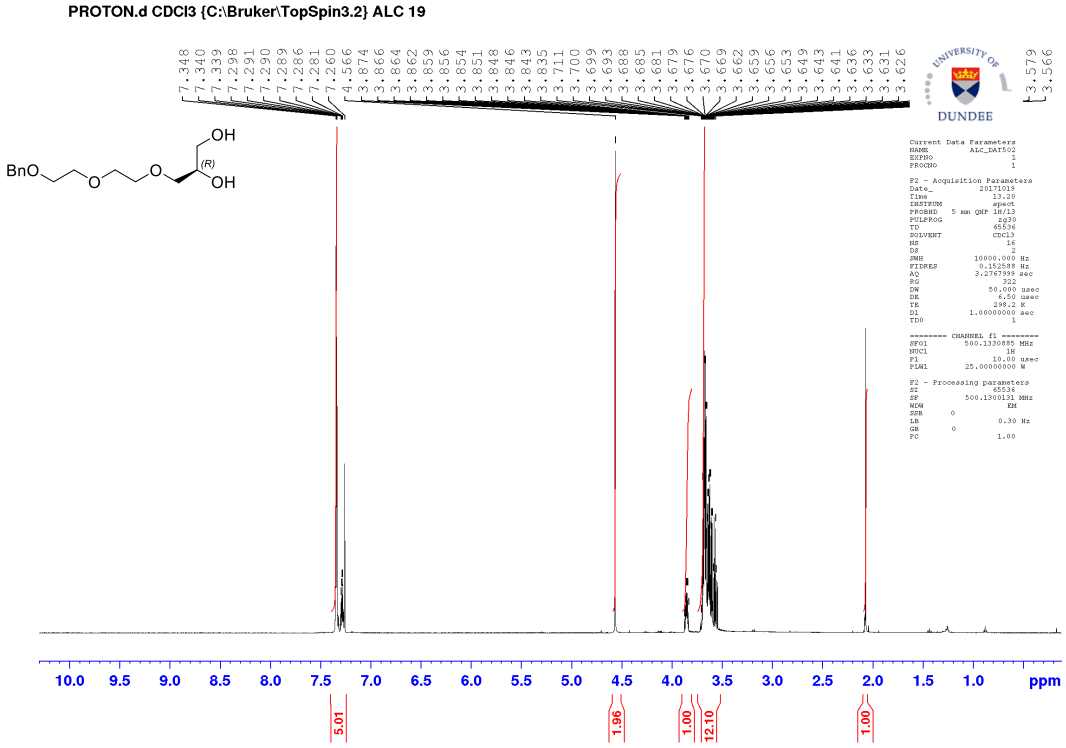

Compound **6**, ^{13}C-NMR $CDCl_3$, 126 MHz

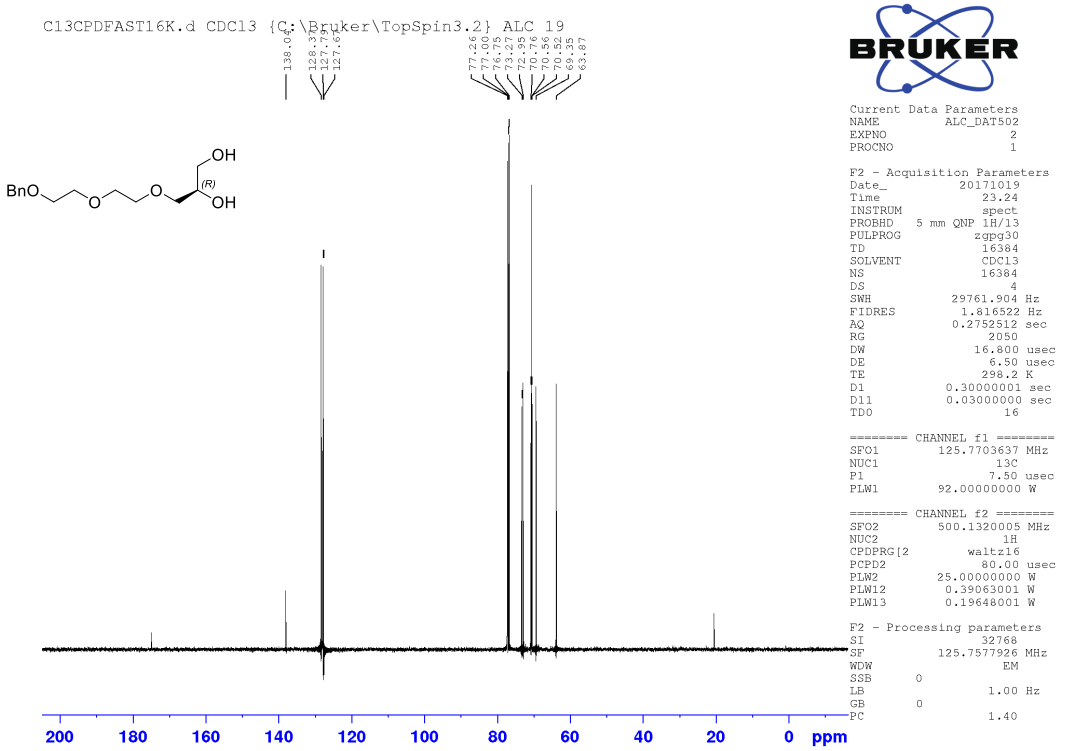

Compound **7**, ^{1}H-NMR $CDCl_3$, 500 MHz

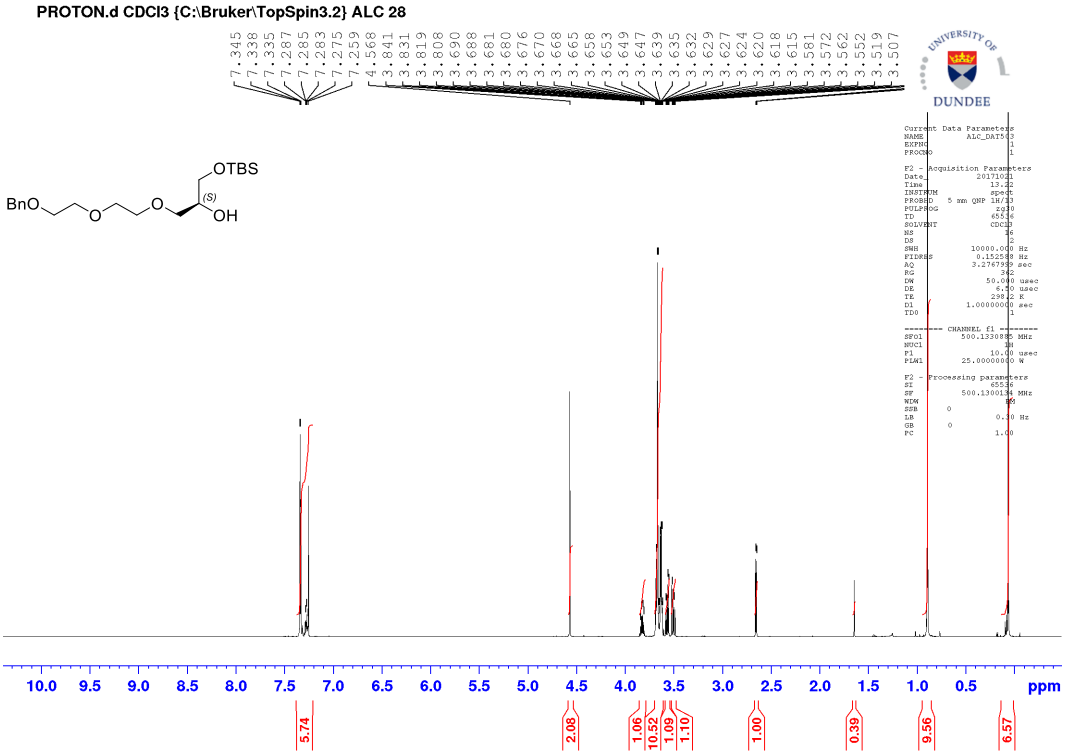

Compound **7**, ^{13}C-NMR $CDCl_3$, 126 MHz

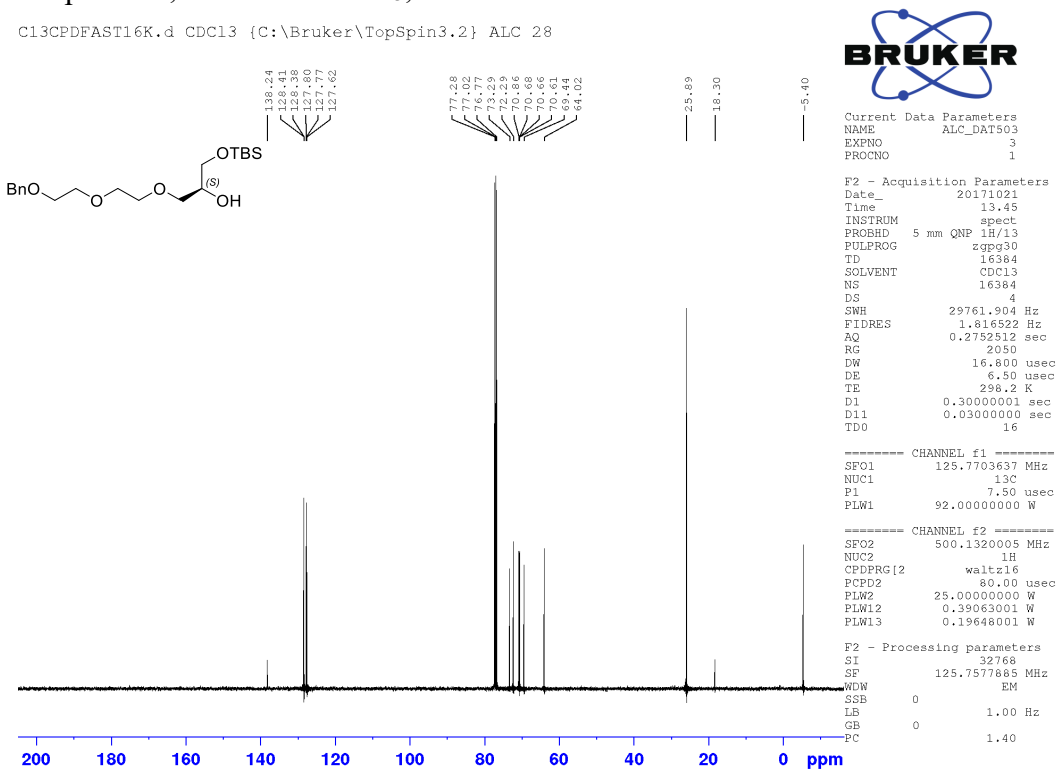

Compound **8**, ^{1}H-NMR $CDCl_3$, 400 MHz

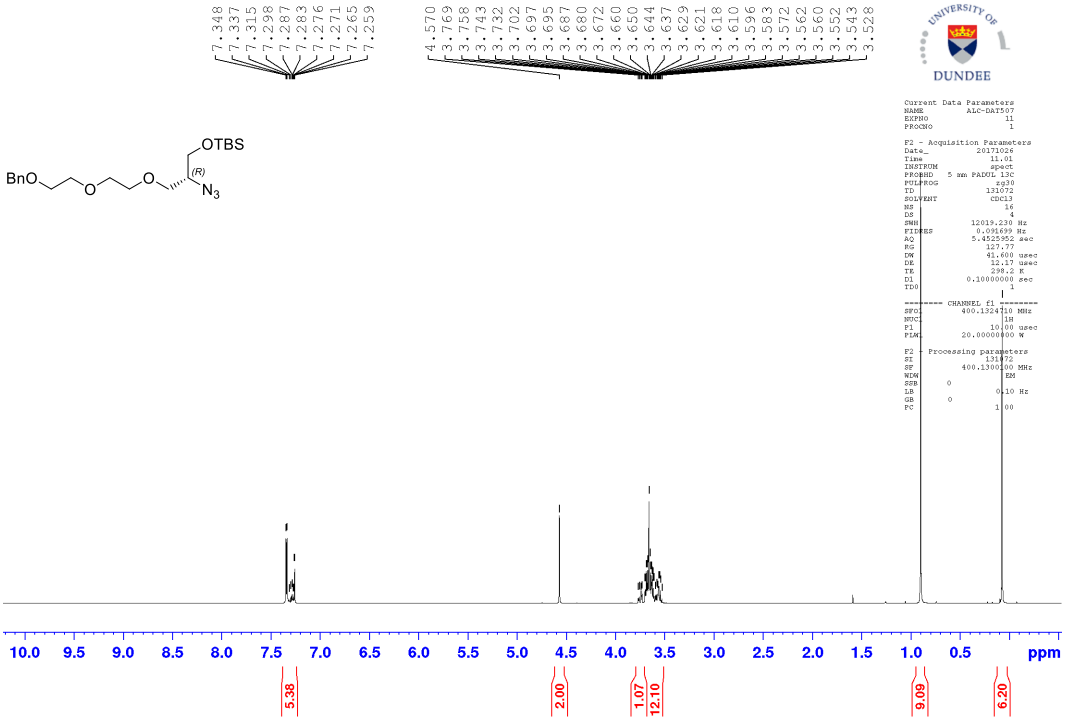

Compound **8**, ^{13}C-NMR $CDCl_3$, 101 MHz

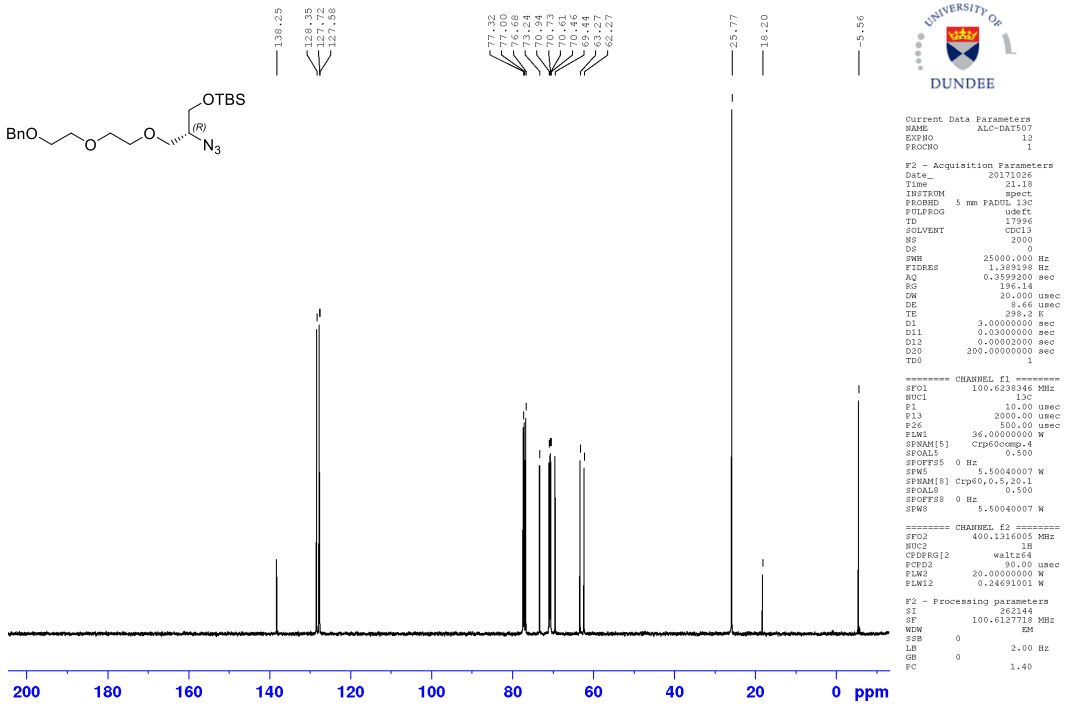

Compound **10**, ^{1}H-NMR $CDCl_3$, 400 MHz

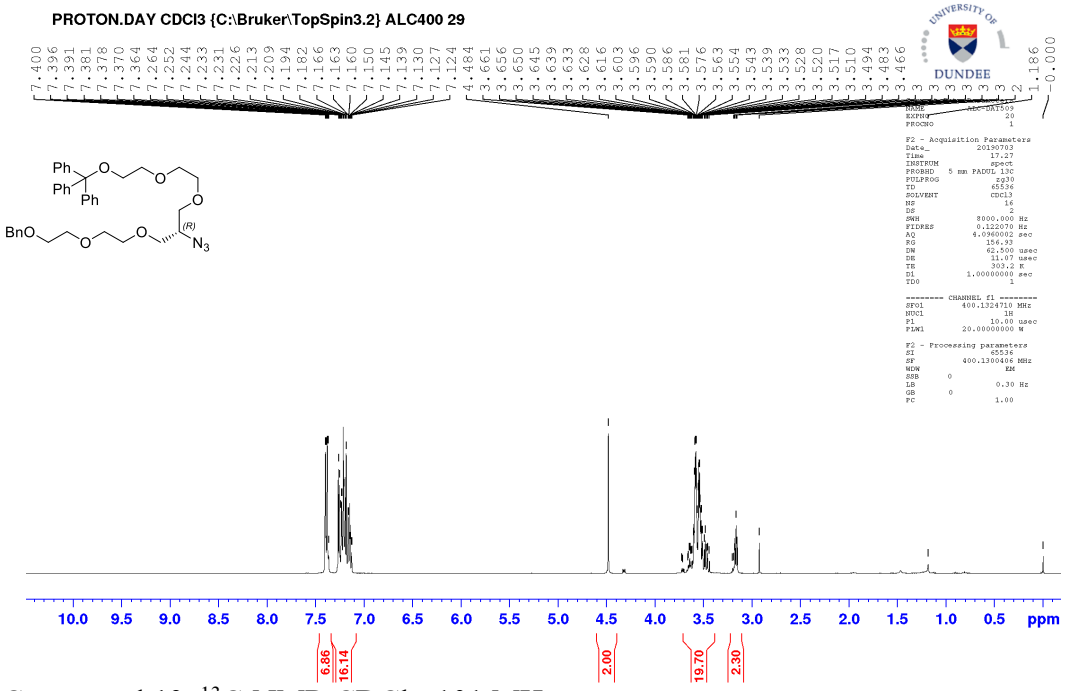

Compound **10**, ^{13}C-NMR $CDCl_3$, 101 MHz

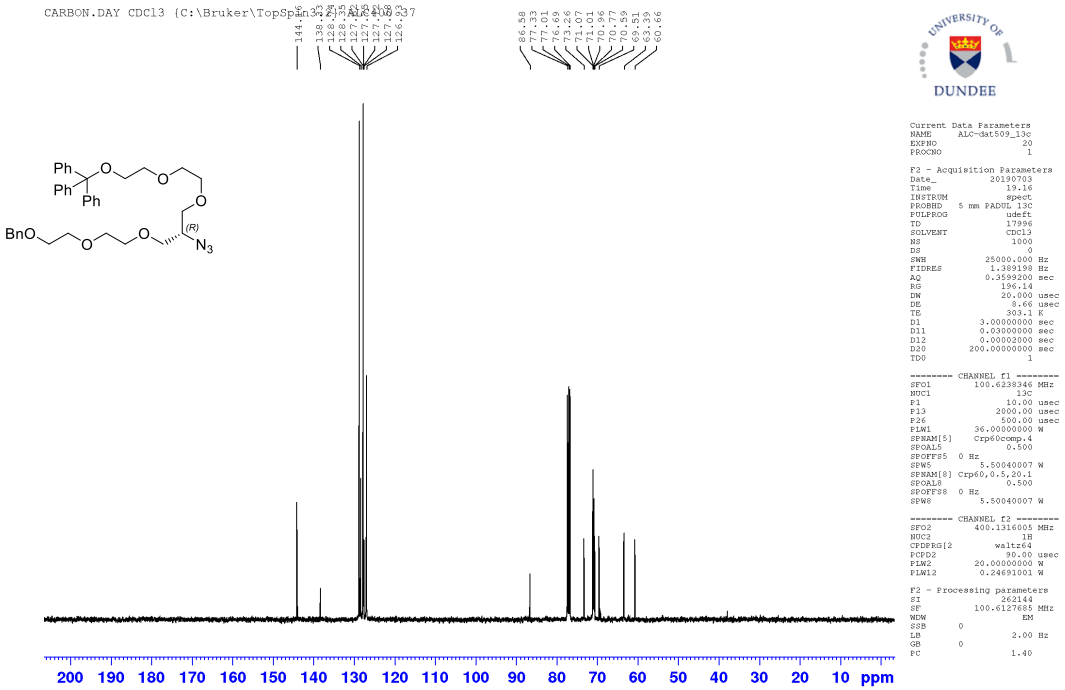

Compound **11**, ^{1}H-NMR $CDCl_3$, 500 MHz

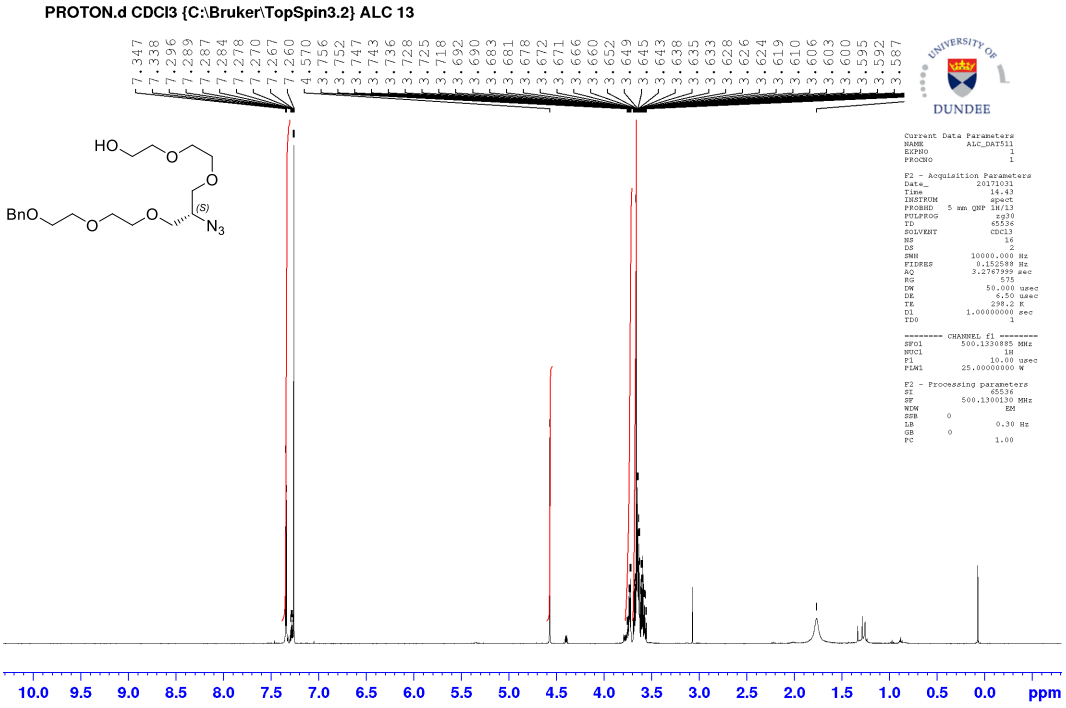

Compound **11**, ^{13}C-NMR $CDCl_3$, 101 MHz

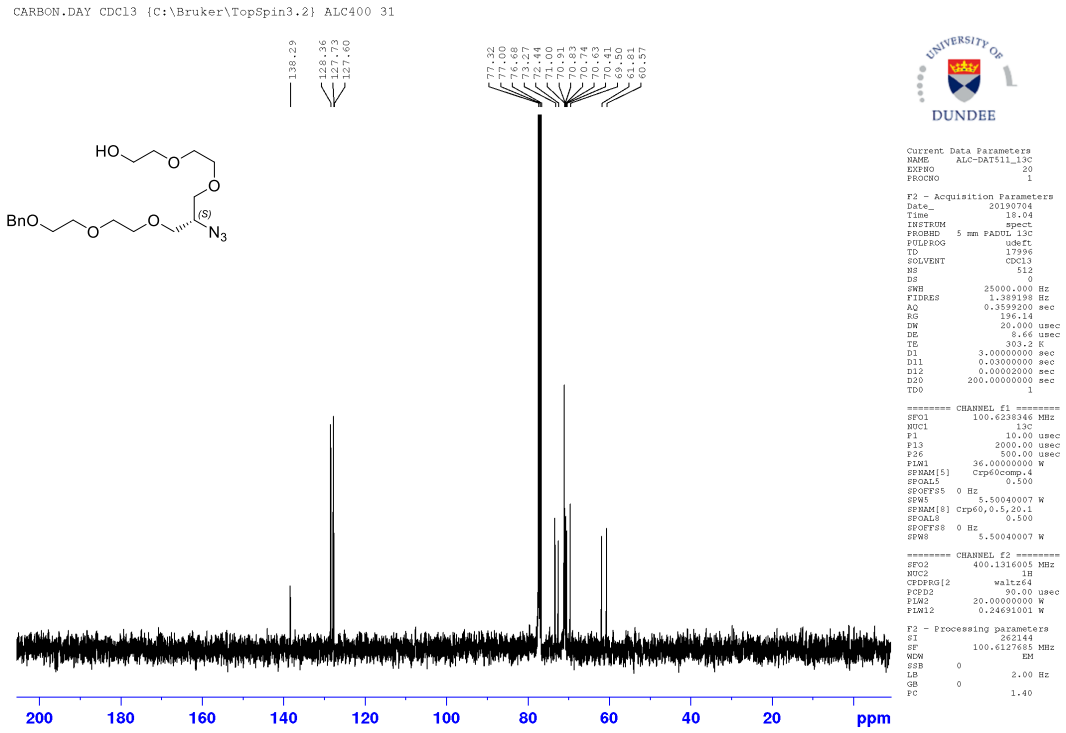

Compound **12**, ^{1}H-NMR $CDCl_3$, 500 MHz

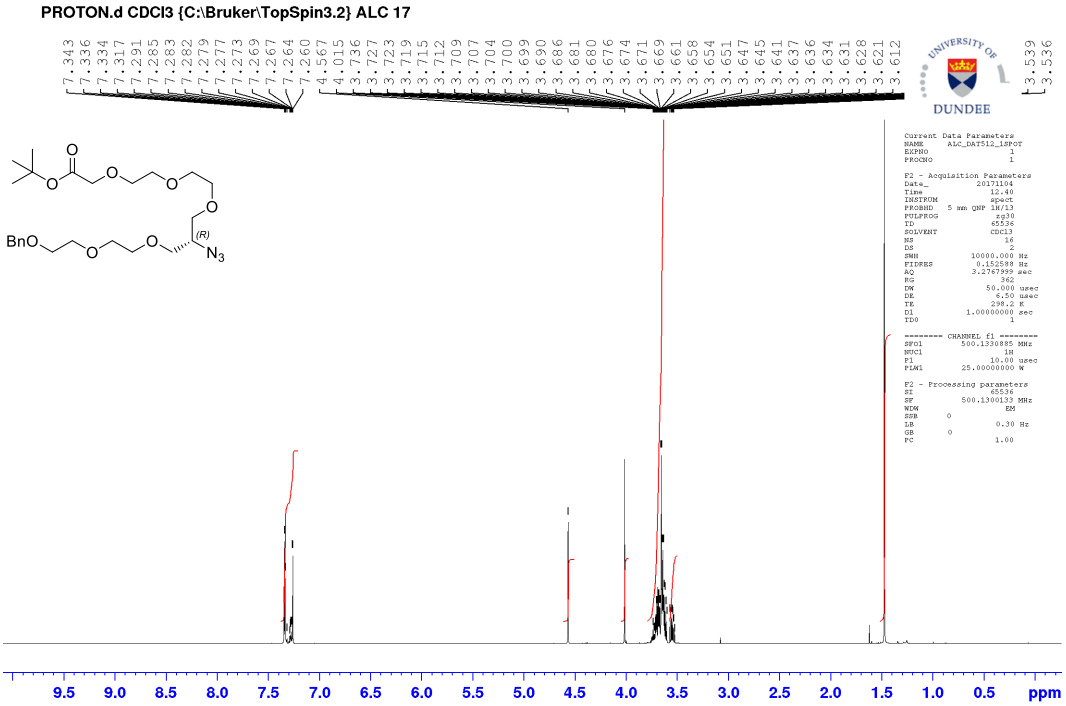

Compound **12**, ^{13}C-NMR $CDCl_3$, 126 MHz

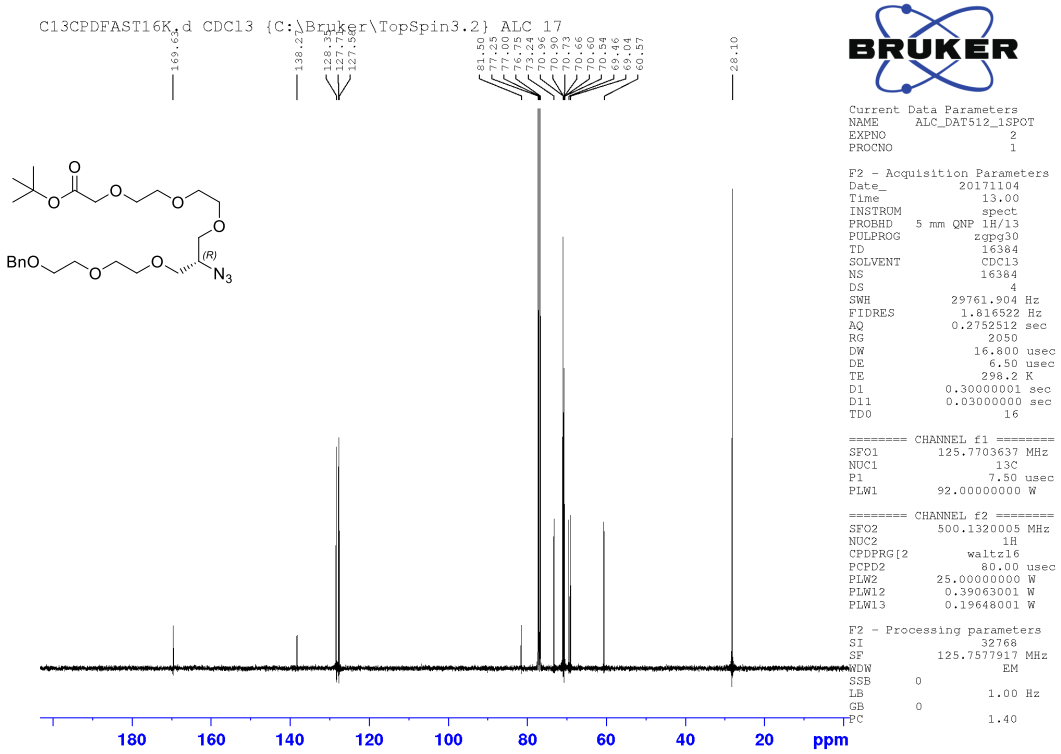

Compound **13**, ^{1}H-NMR $CDCl_3$, 500 MHz

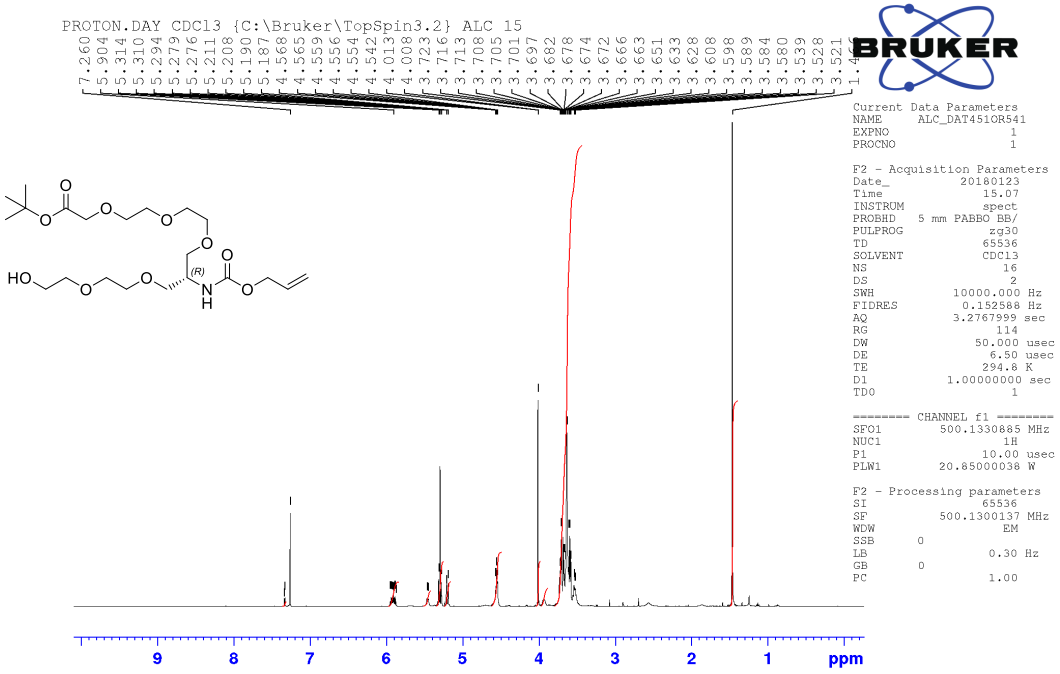

Compound **13**, ^{13}C-NMR $CDCl_3$, 101 MHz

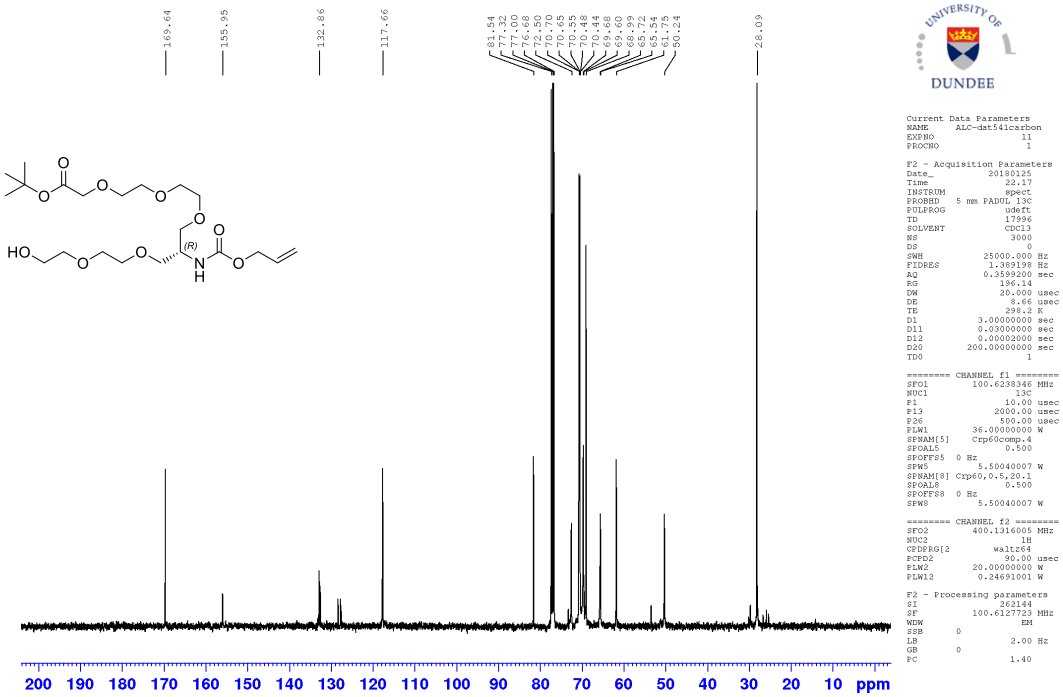

Compound **16**, ^{1}H-NMR MeOD, 400 MHz

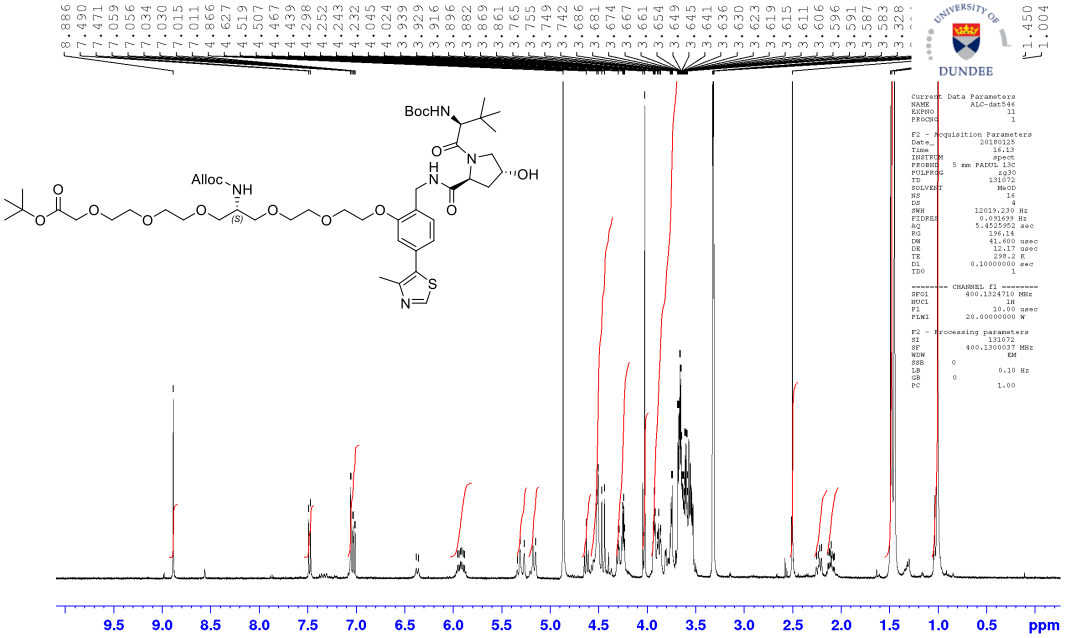

Compound **16**, ^{13}C-NMR MeOD, 101 MHz

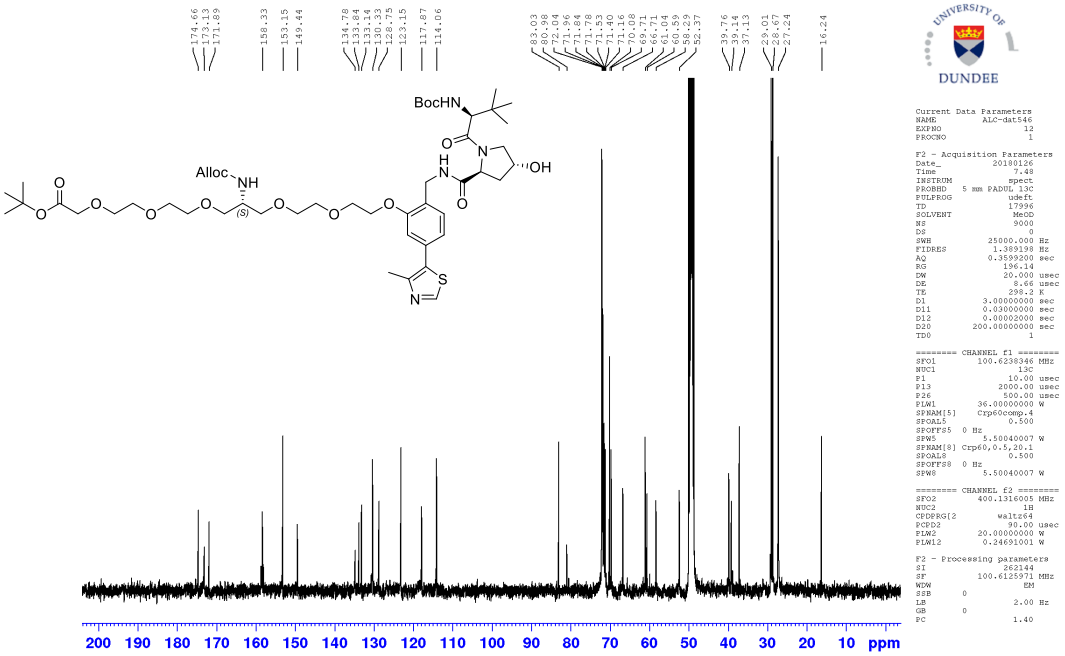

Compound **17**, ^{1}H-NMR MeOD, 400 MHz

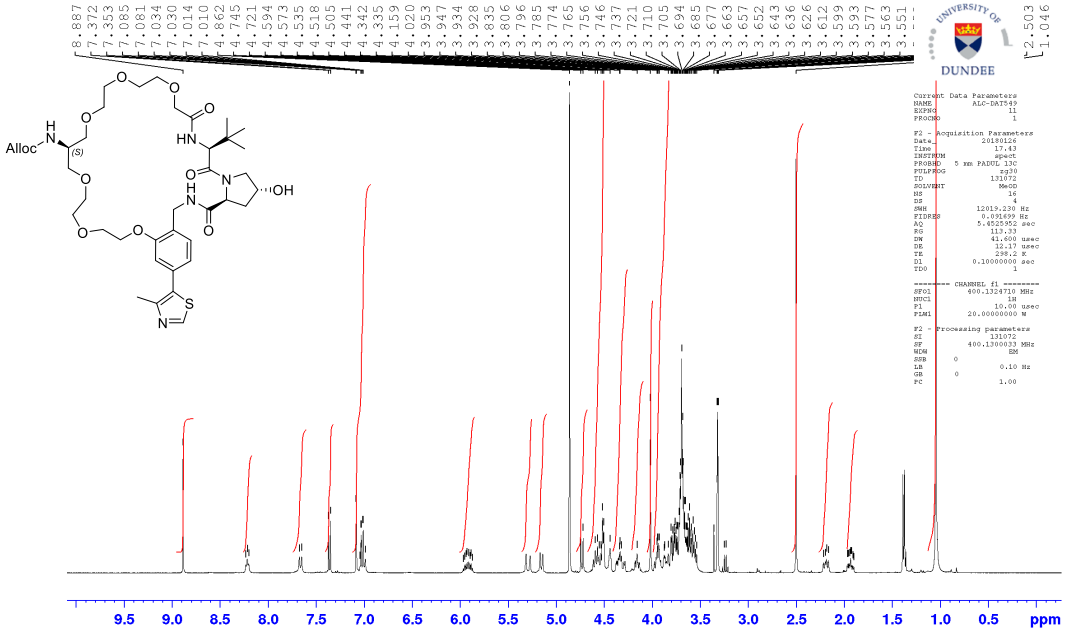

Compound **17**, ^{13}C-NMR MeOD, 101 MHz

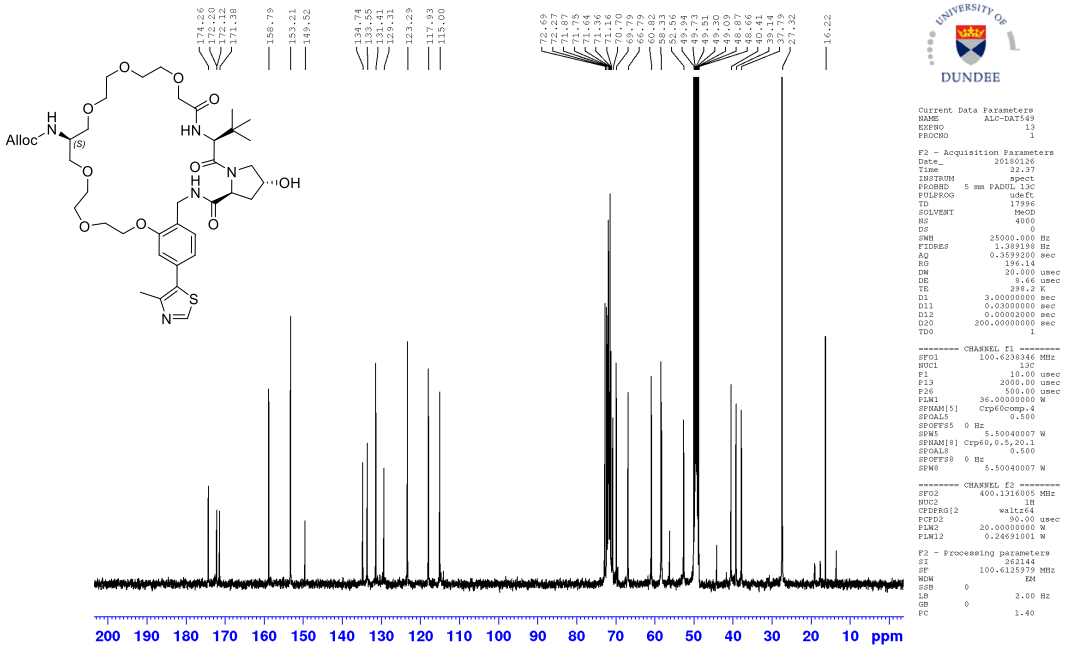

Compound **18**, ^{1}H-NMR DMSO-D6, 400 MHz

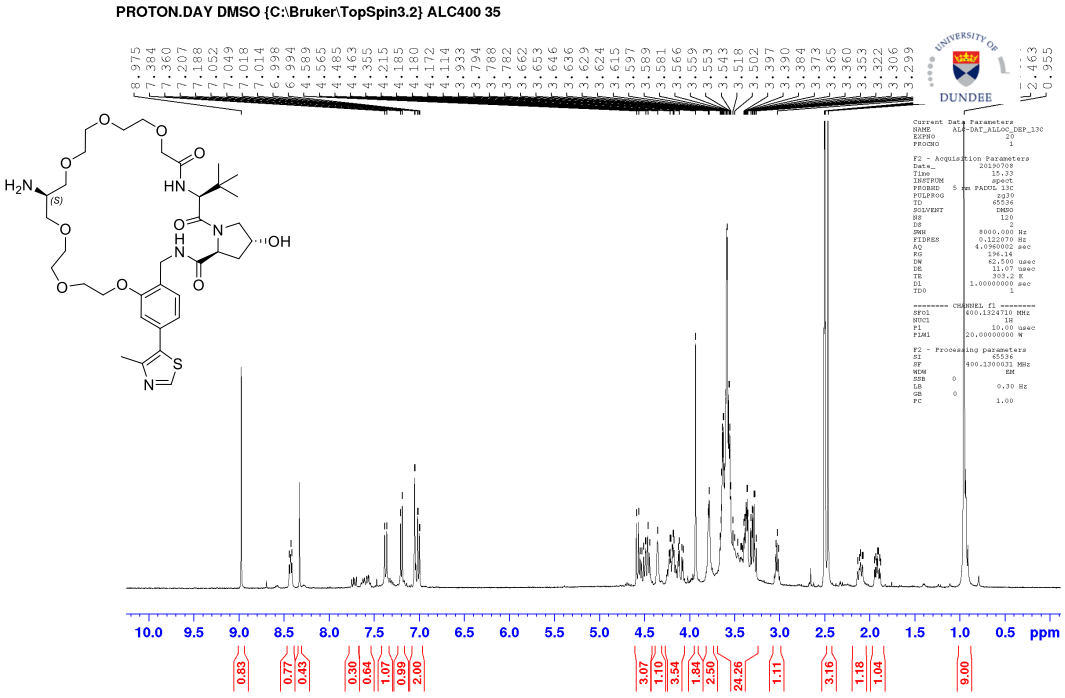

Compound **17**, ^{13}C-NMR DMSO-D6, 101 MHz

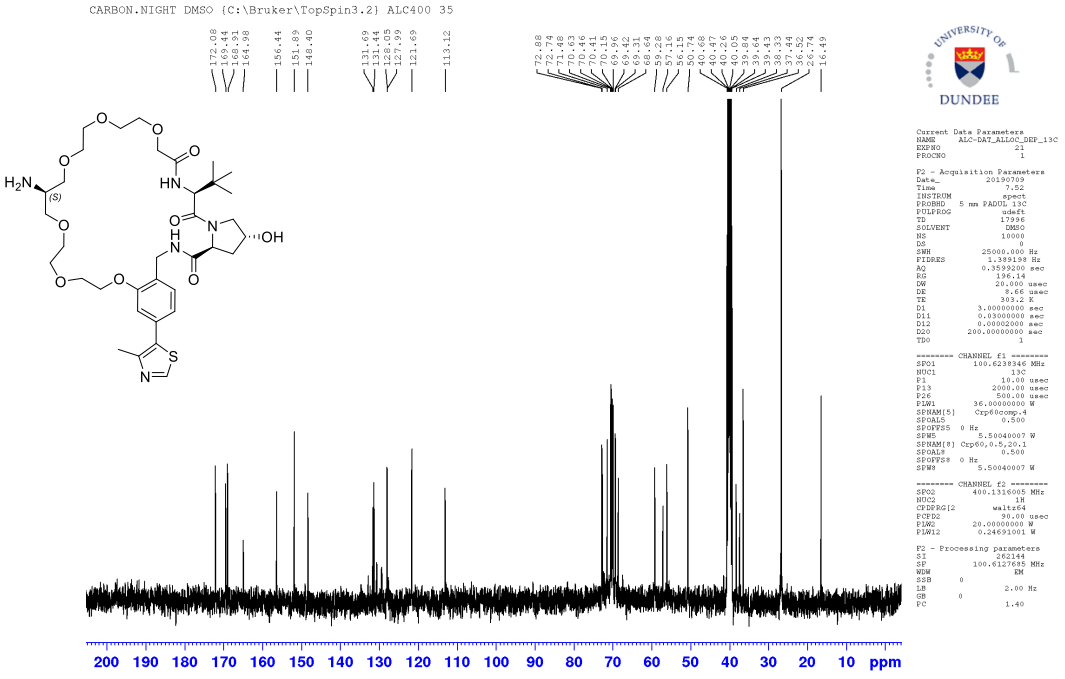

Compound **1**, ^{1}H-NMR MeOD, 400 MHz

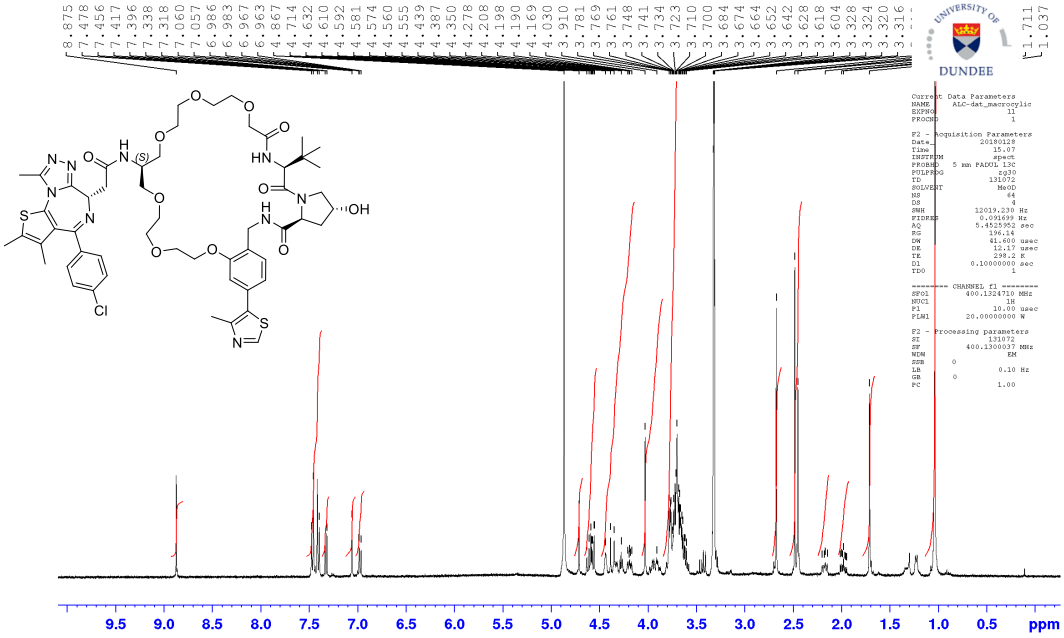

Compound **1**, ^{13}C-NMR MeOD, 101 MHz

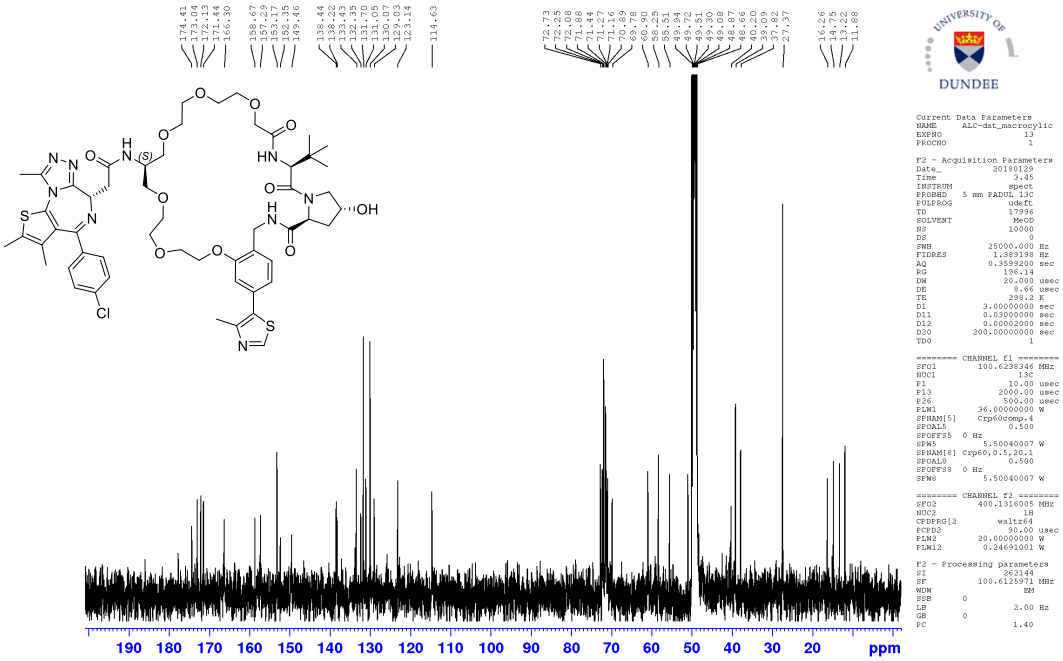

Supplementary References

[1] M. S. Gadd, A. Testa, X. Lucas, K.-H. Chan, W. Chen, D. J. Lamont, M. Zengerle, A. Ciulli, *Nat. Chem. Biol.* **2017**, *13*, 514–521.

[2] C. R. Søndergaard, M. H. M. Olsson, M. Rostkowski, J. H. Jensen, *J. Chem. Theory Comput.* **2011**, *7*, 2284–2295.

[3] E. Harder, W. Damm, J. Maple, C. Wu, M. Reboul, J. Y. Xiang, L. Wang, D. Lupyan, M. K. Dahlgren, J. L. Knight, et al., *J. Chem. Theory Comput.* **2016**, *12*, 281–296.

[4] W. Humphrey, A. Dalke, K. Schulten, *J.Mol.Graphics* **1996**, *14*, 33–8– 27–8.

[5] S. Kawamura, Y. Ito, T. Hirokawa, E. Hikiyama, S. Yamada, S. Shuto, *J. Med. Chem.* **2018**, *61*, 4020–4029.

[6] V. Zoppi, S. J. Hughes, C. Maniaci, A. Testa, T. Gmaschitz, C. Wieshofer, M. Koegl, K. M. Riching, D. L. Daniels, A. Spallarossa, et al., *J. Med. Chem.* **2019**, *62*, 699–726.

[7] M. Zengerle, K.-H. Chan, A. Ciulli, *ACS Chem. Biol.* **2015**, *10*, 1770–1777.

[8] M. J. Roy, S. Winkler, S. J. Hughes, C. Whitworth, M. Galant, W. Farnaby, K. Rumpel, A. Ciulli, *ACS Chem. Biol.* **2019**, *14*, 361–368.

[9] W. Kabsch, *Acta Crystallogr D Biol Crystallogr* **2010**, *66*, 125–132.

[10] P. Evans, *Acta Crystallogr D Biol Crystallogr* **2006**, *62*, 72–82.

[11] M. D. Winn, C. C. Ballard, K. D. Cowtan, E. J. Dodson, P. Emsley, P. R. Evans, R. M. Keegan, E. B. Krissinel, A. G. W. Leslie, A. McCoy, et al., *Acta Crystallogr D Biol Crystallogr* **2011**, *67*, 235–242.

[12] A. J. McCoy, R. W. Grosse-Kunstleve, P. D. Adams, M. D. Winn, L. C. Storoni, R. J. Read, *J Appl Crystallogr* **2007**, *40*, 658–674.

[13] P. Emsley, K. Cowtan, *Acta Crystallogr D Biol Crystallogr* **2004**, *60*, 2126–2132.

[14] G. N. Murshudov, A. A. Vagin, E. J. Dodson, *Acta Crystallogr D Biol Crystallogr* **1997**, *53*, 240–255.

[15] A. W. Schüttelkopf, D. M. F. van Aalten, *Acta Crystallogr D Biol Crystallogr* **2004**, *60*, 1355–1363.

[16] N. W. Moriarty, R. W. Grosse-Kunstleve, P. D. Adams, *Acta Crystallogr D Biol Crystallogr* **2009**, *65*, 1074–1080.

[17] P. D. Adams, P. V. Afonine, G. Bunkoczi, V. B. Chen, I. W. Davis, N. Echols, J. J. Headd, L.-W. Hung, G. J. Kapral, R. W. Grosse-Kunstleve, et al., *Acta Crystallogr D Biol Crystallogr* **2010**, *66*, 213–221.

[18] V. B. Chen, W. B. Arendall, J. J. Headd, D. A. Keedy, R. M. Immormino, G. J. Kapral, L. W. Murray, J. S. Richardson, D. C. Richardson, *Acta Crystallogr D Biol Crystallogr* **2010**, *66*, 12–21.